

An anisotropic mesh adaptation method for the finite element solution of heterogeneous anisotropic diffusion problems

Xianping Li ^{*}

Weizhang Huang [†]

Abstract

Heterogeneous anisotropic diffusion problems arise in the various areas of science and engineering including plasma physics, petroleum engineering, and image processing. Standard numerical methods can produce spurious oscillations when they are used to solve those problems. A common approach to avoid this difficulty is to design a proper numerical scheme and/or a proper mesh so that the numerical solution validates the discrete counterpart (DMP) of the maximum principle satisfied by the continuous solution. A well known mesh condition for the DMP satisfaction by the linear finite element solution of isotropic diffusion problems is the non-obtuse angle condition that requires the dihedral angles of mesh elements to be non-obtuse. In this paper, a generalization of the condition, the so-called anisotropic non-obtuse angle condition, is developed for the finite element solution of heterogeneous anisotropic diffusion problems. The new condition is essentially the same as the existing one except that the dihedral angles are now measured in a metric depending on the diffusion matrix of the underlying problem. Several variants of the new condition are obtained. Based on one of them, two metric tensors for use in anisotropic mesh generation are developed to account for DMP satisfaction and the combination of DMP satisfaction and mesh adaptivity. Numerical examples are given to demonstrate the features of the linear finite element method for anisotropic meshes generated with the metric tensors.

AMS 2010 Mathematics Subject Classification. 65N50, 65N30, 65M50, 65M60

Key words. anisotropic diffusion, anisotropic coefficient, discrete maximum principle, anisotropic mesh generation, anisotropic mesh adaptation, finite element, mesh adaptation

1 Introduction

We are concerned with the numerical solution of the diffusion equation

$$-\nabla \cdot (\mathbb{D} \nabla u) = f, \quad \text{in } \Omega \quad (1)$$

subject to the Dirichlet boundary condition

$$u = g, \quad \text{on } \partial\Omega \quad (2)$$

^{*}Department of Mathematics, the University of Kansas, Lawrence, KS 66045, U.S.A. (lxp@math.ku.edu)

[†]Department of Mathematics, the University of Kansas, Lawrence, KS 66045, U.S.A. (huang@math.ku.edu)

where $\Omega \subset \mathbb{R}^d$ ($d = 1, 2$, or 3) is the physical domain, f and g are given functions, and $\mathbb{D} = \mathbb{D}(\mathbf{x})$ is the diffusion matrix assumed to be symmetric and strictly positive definite on Ω . The boundary value problem (BVP) (1) and (2) becomes a heterogeneous anisotropic diffusion problem when \mathbb{D} changes from place to place (heterogeneous) and its eigenvalues are not all equal (anisotropic) at least on a portion of Ω . When a standard numerical method, such as a finite element, a finite difference, or a finite volume method, is used to solve this problem, spurious oscillations can occur in the computed solution. A challenge is then to design a proper numerical scheme and/or a proper mesh so that the computed solution is free of spurious oscillations. In some applications such as plasma physics, it is further desired that the mesh be aligned with the fast diffusion direction so that no excessive numerical dissipation is introduced in slow diffusion directions. Moreover, mesh adaptation is often necessary for improving computational efficiency and accuracy when the physical solution and/or the diffusion matrix have sharp jumps.

Anisotropic diffusion problems arise in the various areas of science and engineering including plasma physics in fusion experiments and astrophysics [25, 26, 27, 55, 61, 63], petroleum reservoir simulation [1, 2, 16, 22, 53], and image processing [12, 13, 39, 54, 57, 69]. In plasma physics, magnetized plasmas are constrained to move primarily along magnetic field lines. Their heat conductivity in the direction parallel to the magnetic field is much higher than those perpendicular to it, and the ratio of the conduction coefficients can easily exceed 10^{10} in fusion experiments. The numerical simulation of the heat conduction of plasmas must not only produce a physically meaningful temperature distribution but also avoid excessive numerical dissipation in the directions perpendicular to the magnetic field. In petroleum engineering, fluids such as water, crude oil, and natural gas are stored in reservoir rocks filled by interconnected networks of pores. The diffusion and flow of those fluids depend crucially on the rocks' permeability which changes with location and flow direction and has much large values in horizontal directions than in the vertical direction. Finally, PDE-based anisotropic diffusion filters have been successfully used for shape recognition and edge detection in image processing.

The BVP (1) and (2) is a representative example of anisotropic diffusion problems arising in those areas. As typical for diffusion problems, it satisfies the maximum principle

$$\max_{\mathbf{x} \in \Omega \cup \partial\Omega} u(\mathbf{x}) \leq \max\{0, \max_{\mathbf{s} \in \partial\Omega} g(\mathbf{s})\} \quad (3)$$

provided that $f(\mathbf{x}) \leq 0$ holds for all $\mathbf{x} \in \Omega$. The BVP has been studied extensively in the past, and a major effort has been made to avoid spurious oscillations in the numerical solution. A common strategy is to develop numerical schemes satisfying the discrete counterpart of (3) – the so-called discrete maximum principle (DMP), which are known to produce numerical solutions free of spurious oscillations [14, 68]. The studies can be traced back to early works by Varga [68], Ciarlet [14], Ciarlet and Raviart [15], and Stoyan [64, 65] where a number of sufficient conditions in a general and abstract setting are obtained for a class of linear elliptic partial differential equations (PDEs). For example, denote by $A\mathbf{u} = \mathbf{f}$ the linear algebraic system resulting from the application of a numerical scheme to a linear elliptic PDE supplemented with a Dirichlet boundary condition, where A is the $n \times n$ stiffness matrix, \mathbf{u} is the unknown vector, and \mathbf{f} the right-hand-side vector. Then, a sufficient condition is given as follows.

Lemma 1.1 ([65]) *If the stiffness matrix A satisfies*

- (a) *that A is monotone with $A^{(-)}$ being either nonsingular, or singular and irreducible; and* (4)
- (b) *that $A^{(-)}\mathbf{e}^{(n)} \geq 0$,* (5)

then the numerical scheme satisfies DMP.

Here, matrix A is said to be monotone if A is nonsingular and $A^{-1} \geq 0$ (i.e., all entries of A^{-1} are non-negative), and $A^{(-)}$ and $\mathbf{e}^{(n)}$ are defined as

$$a_{ij}^{(-)} = \begin{cases} a_{ii}, & \text{for } i = j \\ a_{ij}, & \text{for } i \neq j, a_{ij} \leq 0, \\ 0, & \text{for } i \neq j, a_{ij} > 0 \end{cases}, \quad \mathbf{e}^{(n)} = \begin{bmatrix} 1 \\ \vdots \\ 1 \end{bmatrix}. \quad (6)$$

Note that condition (5) is equivalent to that $A^{(-)}$ has nonnegative row sums. Moreover, $A = A^{(-)}$ and the condition (4) holds when A is an M -matrix [67]. From Lemma 1.1 we have the following lemma.

Lemma 1.2 *If the stiffness matrix A is an M -matrix and has nonnegative row sums, then the numerical scheme satisfies DMP.*

Numerical schemes satisfying DMP have been developed along the line of those sufficient conditions by either designing a proper discretization for the underlying PDE or employing a suitable mesh. To date most success has been made for the isotropic diffusion case where \mathbb{D} is in the scalar matrix form, $\mathbb{D} = a(\mathbf{x})I$, with $a(\mathbf{x})$ being a scalar function; e.g., see [9, 10, 15, 36, 37, 38, 44, 49, 66, 71]. In particular, it is shown in [9, 15] that the linear finite element method (FEM) satisfies DMP when the mesh is simplicial and satisfies the so-called non-obtuse angle condition requiring that the dihedral angles of all mesh elements be non-obtuse. In two dimensions this condition can be replaced by a weaker condition (the Delaunay condition) that the sum of any pair of angles opposite a common edge is less than or equal to π [49, 66]. Similar mesh conditions are developed in [36, 37, 38, 44] for elliptic problems with a nonlinear diffusion coefficient in the form $\mathbb{D} = a(\mathbf{x}, u, \nabla u)I$ and with mixed boundary conditions. Burman and Ern [10] propose a nonlinear stabilized Galerkin approximation for the Laplace operator and prove that it satisfies DMP on arbitrary meshes and for arbitrary space dimension without resorting to the non-obtuse angle condition.

On the other hand, the anisotropic diffusion case is more difficult and only limited success has been made [16, 18, 25, 26, 27, 43, 46, 47, 48, 50, 51, 52, 53, 61]. For example, Drăgănescu et al. [18] show that the non-obtuse angle condition fails to guarantee DMP satisfaction in the anisotropic diffusion case. The techniques proposed by Liska and Shashkov [52] and Kuzmin et al. [43] to locally modify (or repair) the underlying numerical scheme, by Sharma and Hammett [61] to employ slope limiters in the discretization of the PDE, by Mlacnik and Durlofsky [53] to optimize the mesh for a multipoint flux approximation (MPFA) finite volume method (e.g., see [1, 2] for the method), and by Li et al. [50] to optimize a triangular mesh for the finite element solution, help reduce spurious oscillations. A nonlinear, first order finite volume method developed by Le Potier [46, 47] and further improved by Lipnikov et al. [51] gives rise to a stiffness M -matrix on arbitrary

meshes when applied to parabolic PDEs but fails to satisfy DMP when applied to steady-state elliptic problems. A first order finite difference method having similar features is proposed by Le Potier [48].

In this paper we study the linear finite element solution of BVP (1) and (2) with a general diffusion matrix $\mathbb{D} = \mathbb{D}(\mathbf{x})$. The objective is threefold. The first is to develop a generalization of the well known non-obtuse angle condition, the so-called anisotropic non-obtuse angle condition (cf. equation (24)), so that the linear FEM satisfies DMP when the mesh is simplicial and satisfies this condition. The condition requires that the dihedral angles of all mesh elements, measured in a metric depending on \mathbb{D} , be non-obtuse. It reduces to the non-obtuse angle condition for isotropic diffusion matrices. It also reproduces several existing mesh conditions for homogeneous anisotropic media for which \mathbb{D} is a full, constant matrix (see Remark 2.2). The second objective is to derive a metric tensor for use in mesh generation based on the anisotropic non-obtuse angle condition. This is done by adopting the so-called M -uniform mesh approach [31] where an anisotropic mesh is generated as an M -uniform mesh or a uniform mesh in the metric specified by a tensor. M -uniform meshes generated with the metric tensor satisfy the anisotropic non-obtuse angle condition and are aligned with the diffusion matrix \mathbb{D} (cf. §3). The final objective is to combine both mesh adaptivity and DMP satisfaction in the numerical solution of anisotropic diffusion problems. An optimal metric tensor (see (55)) accounting for both considerations is obtained by minimizing an interpolation error bound, and advantages of using adaptive, DMP-bound meshes are demonstrated in numerical examples. To the authors' best knowledge, this is the first effort that mesh adaptivity and DMP satisfaction are considered simultaneously in the numerical solution of anisotropic diffusion problems.

The outline of this paper is as follows. In section 2, the linear finite element solution of (1) and (2) is described and the anisotropic non-obtuse angle condition and several variants are derived. Section 3 is devoted to the derivation of the metric tensor based on the anisotropic non-obtuse angle condition. In section 4, the combination of mesh adaptation and DMP satisfaction is addressed, and an optimal metric tensor is obtained by minimizing an interpolation error bound. Numerical examples are presented in section 5. Finally, section 6 contains conclusions and comments.

2 Anisotropic non-obtuse angle conditions for linear finite element approximation

Consider the linear finite element solution of BVP (1) and (2). Assume that Ω is a connected polygon or polyhedron and an affine family of simplicial triangulations $\{\mathcal{T}_h\}$ is given thereon. Let

$$U_g = \{v \in H^1(\Omega) \mid v|_{\partial\Omega} = g\}.$$

Denote by $U_g^h \subset U_g$ the linear finite element space associated with mesh \mathcal{T}_h . Then a linear finite element solution $\tilde{u}^h \in U_g^h$ to BVP (1) and (2) is defined by

$$\int_{\Omega} (\nabla v^h)^T \mathbb{D} \nabla \tilde{u}^h d\mathbf{x} = \int_{\Omega} f v^h d\mathbf{x}, \quad \forall v^h \in U_0^h \quad (7)$$

where $U_0^h = U_g^h$ with $g = 0$. This equation can be rewritten as

$$\sum_{K \in \mathcal{T}_h} \int_K (\nabla v^h)^T \mathbb{D} \nabla \bar{u}^h d\mathbf{x} = \sum_{K \in \mathcal{T}_h} \int_K f v^h d\mathbf{x}, \quad \forall v^h \in U_0^h. \quad (8)$$

Generally speaking, the integrals in (8) cannot be carried out analytically, and numerical quadrature is needed. We assume that a quadrature rule has been chosen on the reference element \hat{K} for this purpose,

$$\int_{\hat{K}} v(\xi) d\xi \approx |\hat{K}| \sum_{k=1}^m \hat{w}_k v(\hat{b}_k), \quad \sum_{k=1}^m \hat{w}_k = 1, \quad (9)$$

where \hat{w}_k 's are the weights and \hat{b}_k 's the quadrature nodes. A 2D example of such quadrature rules is given by $\hat{w}_k = \frac{1}{3}$ ($k = 1, 2, 3$) and the barycentric coordinates of the nodes $(\frac{1}{6}, \frac{1}{6}, \frac{2}{3})$, $(\frac{1}{6}, \frac{2}{3}, \frac{1}{6})$, and $(\frac{2}{3}, \frac{1}{6}, \frac{1}{6})$; and a 3D example is $\hat{w}_i = \frac{1}{4}$ ($i = 1, 2, 3, 4$) and the barycentric coordinates of the nodes $(a, a, a, 1 - 3a)$, $(a, a, 1 - 3a, a)$, $(a, 1 - 3a, a, a)$, and $(1 - 3a, a, a, a)$ with $a = \frac{5-\sqrt{5}}{20}$; e.g., see [21].

Let F_K be the affine mapping from \hat{K} to K such that $K = F_K(\hat{K})$, and denote $b_k^K = F_K(\hat{b}_k)$, $k = 1, \dots, m$. Upon applying (9) to the integrals in (8) and changing variables, the finite element approximation problem becomes seeking $u^h \in U_g^h$ such that

$$\sum_{K \in \mathcal{T}_h} |K| \sum_{k=1}^m \hat{w}_k (\nabla v^h|_K)^T \mathbb{D}(b_k^K) \nabla u^h|_K = \sum_{K \in \mathcal{T}_h} |K| \sum_{k=1}^m \hat{w}_k f(b_k^K) v^h(b_k^K), \quad \forall v^h \in U_0^h \quad (10)$$

where $\nabla v^h|_K$ and $\nabla u^h|_K$ denote the restriction of ∇v^h and ∇u^h on K , respectively. Note that we have used in (10) the fact that $\nabla v^h|_K$ and $\nabla u^h|_K$ are constant. Letting

$$\mathbb{D}_K = \sum_{k=1}^m \hat{w}_k \mathbb{D}(b_k^K), \quad (11)$$

we can rewrite (10) into

$$\sum_{K \in \mathcal{T}_h} |K| (\nabla v^h|_K)^T \mathbb{D}_K \nabla u^h|_K = \sum_{K \in \mathcal{T}_h} |K| \sum_{k=1}^m \hat{w}_k f(b_k^K) v^h(b_k^K), \quad \forall v^h \in U_0^h. \quad (12)$$

We now express (12) in a matrix form. Denote the numbers of the elements, vertices, and interior vertices of \mathcal{T}_h by N , N_v , and N_{vi} , respectively. Assume that the vertices are ordered in such a way that the first N_{vi} vertices are the interior vertices. Then U_0^h and u^h can be expressed as

$$U_0^h = \text{span}\{\phi_1, \dots, \phi_{N_{vi}}\} \quad (13)$$

and

$$u^h = \sum_{j=1}^{N_{vi}} u_j \phi_j + \sum_{j=N_{vi}+1}^{N_v} u_j \phi_j, \quad (14)$$

where ϕ_j is the linear basis function associated with the j -th vertex, \mathbf{a}_j . Note that the boundary condition (2) can be approximated by

$$u_j = g_j \equiv g(\mathbf{a}_j), \quad j = N_{vi} + 1, \dots, N_v. \quad (15)$$

Substituting (14) into and taking $v^h = \phi_i$ ($i = 1, \dots, N_{vi}$) in (12) and combining the resulting equations with (15), we obtain the linear algebraic system

$$A \mathbf{u} = \mathbf{f}, \quad (16)$$

where

$$A = \begin{bmatrix} A_{11} & A_{12} \\ 0 & I \end{bmatrix}, \quad (17)$$

I is the identity matrix of size $(N_v - N_{vi})$, and

$$\mathbf{u} = (u_1, \dots, u_{N_{vi}}, u_{N_{vi}+1}, \dots, u_{N_v})^T,$$

$$\mathbf{f} = (f_1, \dots, f_{N_{vi}}, g_{N_{vi}+1}, \dots, g_{N_v})^T.$$

The entries of the stiffness matrix A and the right-hand-side vector \mathbf{f} are given by

$$a_{ij} = \sum_{K \in \mathcal{T}_h} |K| (\nabla \phi_i|_K)^T \mathbb{D}_K \nabla \phi_j|_K, \quad i = 1, \dots, N_{vi}, \quad j = 1, \dots, N_v, \quad (18)$$

$$f_i = \sum_{K \in \mathcal{T}_h} |K| \sum_{k=1}^m \hat{w}_k f(b_k^K) \phi_i(b_k^K), \quad i = 1, \dots, N_{vi}. \quad (19)$$

We recall that (16) and (17) have been obtained under the Dirichlet boundary condition (2). It is not difficult to show that a linear system in the same form can be obtained for mixed boundary conditions provided that $\Gamma_D \neq \emptyset$, with Γ_D being the part of the boundary where the Dirichlet condition is imposed. Therefore, the mesh conditions developed below also work for mixed boundary conditions with $\Gamma_D \neq \emptyset$.

We now study under what mesh conditions the scheme (16) satisfies DMP. Our basic tool is Lemma 1.2, i.e., we show that A is an M -matrix and has non-negative row sums when the mesh satisfies the condition (24) below. To this end, we first introduce some notation. Denote the vertices of K by $\mathbf{a}_1^K, \mathbf{a}_2^K, \dots, \mathbf{a}_{d+1}^K$. The edge matrix of K is defined as

$$E_K = [\mathbf{a}_2^K - \mathbf{a}_1^K, \mathbf{a}_3^K - \mathbf{a}_1^K, \dots, \mathbf{a}_{d+1}^K - \mathbf{a}_1^K].$$

From the definition of simplices, E_K is nonsingular [62]. Then, a set of \mathbf{q} -vectors (cf. Fig. 1) can be defined as

$$[\mathbf{q}_2^K, \mathbf{q}_3^K, \dots, \mathbf{q}_{d+1}^K] = E_K^{-T}, \quad \mathbf{q}_1^K = -\sum_{i=2}^{d+1} \mathbf{q}_i^K. \quad (20)$$

This set of vectors has the following properties.

(i) By definition, it follows that

$$\begin{aligned} \mathbf{q}_i^K \cdot (\mathbf{a}_j^K - \mathbf{a}_1^K) &= \delta_{ij}, & i = 2, \dots, d+1; \quad j = 1, \dots, d+1 \\ \mathbf{q}_1^K \cdot (\mathbf{a}_j^K - \mathbf{a}_i^K) &= \delta_{1j}, \end{aligned} \quad (21)$$

where δ_{ij} is the Kronecker delta function.

(ii) Denote by \mathbf{S}_i^K the face opposite to vertex \mathbf{a}_i^K (i.e., the face not having \mathbf{a}_i as a vertex). Then (21) implies that \mathbf{q}_i^K is the inward normal to the face \mathbf{S}_i^K ; see Fig. 1.

- (iii) The dihedral angle, α_{ij} , between any two faces \mathbf{S}_i^K and \mathbf{S}_j^K ($i \neq j$) is defined as the supplement of the angle between the inward normals to the faces. It can be calculated by

$$\cos(\alpha_{ij}) = -\frac{\mathbf{q}_i^K \cdot \mathbf{q}_j^K}{\|\mathbf{q}_i^K\| \|\mathbf{q}_j^K\|}, \quad i \neq j. \quad (22)$$

- (iv) It is known [8, 44] that, for any vertex of K with the global and local indices i and i_K , respectively, there holds

$$\nabla \phi_i|_K = \mathbf{q}_{i_K}^K. \quad (23)$$

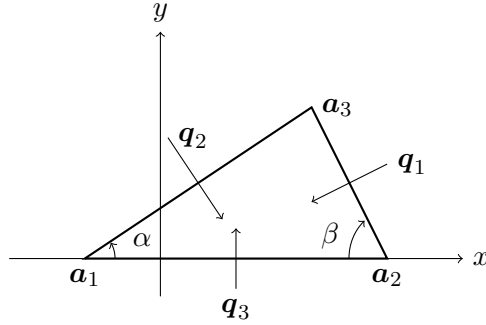


Figure 1: A sketch of the \mathbf{q} vectors for an arbitrary element. The angles sharing the edge connecting vertices \mathbf{a}_1 and \mathbf{a}_2 are α and β .

The main result of this section is stated in the following theorem.

Theorem 2.1 *If the mesh satisfies the anisotropic non-obtuse angle condition*

$$(\mathbf{q}_i^K)^T \mathbb{D}_K \mathbf{q}_j^K \leq 0, \quad \forall i \neq j, \quad i, j = 1, 2, \dots, d+1, \quad \forall K \in \mathcal{T}_h \quad (24)$$

then the linear finite element scheme (12) for solving BVP (1) and (2) satisfies DMP.

Proof. We prove this theorem using Lemma 1.2. That is, we show that the stiffness matrix A has non-negative row sums and is an M -matrix when the mesh satisfies condition (24).

(i) We first show that A has non-negative row sums. From (17) we only need to show $\sum_{j=1}^{N_v} a_{ij} \geq 0$ for $i = 1, \dots, N_v$. From (18) we have

$$\begin{aligned} \sum_{j=1}^{N_v} a_{ij} &= \sum_{j=1}^{N_v} \sum_{K \in \mathcal{T}_h} |K| (\nabla \phi_i|_K)^T \mathbb{D}_K \nabla \phi_j|_K \\ &= \sum_{K \in \mathcal{T}_h} |K| (\nabla \phi_i|_K)^T \mathbb{D}_K \nabla \left(\sum_{j=1}^{N_v} \phi_j \right) \Big|_K \\ &= 0, \end{aligned} \quad (25)$$

where we have used the fact that $\sum_{j=1}^{N_v} \phi_j(\mathbf{x}) \equiv 1$ for any $\mathbf{x} \in K$.

(ii) Next we show that

$$a_{ij} \leq 0, \quad \forall i \neq j, i, j = 1, \dots, N_v \quad (26)$$

$$a_{ii} \geq 0, \quad \forall i = 1, \dots, N_v. \quad (27)$$

Let ω_i (or ω_j) be the patch of the elements containing \mathbf{a}_i (or \mathbf{a}_j) as a vertex. Notice that $\nabla \phi_i|_K = 0$ when $K \notin \omega_i$. Denote the local indices of vertices \mathbf{a}_i and \mathbf{a}_j on K by i_K and j_K , respectively. Then from (18), (23), and (24), we have, for $i \neq j$, $i = 1, \dots, N_{vi}$, $j = 1, \dots, N_v$,

$$\begin{aligned} a_{ij} &= \sum_{K \in \omega_i \cap \omega_j} |K| (\nabla \phi_i|_K)^T \mathbb{D}_K \nabla \phi_j|_K \\ &= \sum_{K \in \omega_i \cap \omega_j} |K| (\mathbf{q}_{i_K}^K)^T \mathbb{D}_K \mathbf{q}_{j_K}^K \end{aligned} \quad (28)$$

$$\leq 0. \quad (29)$$

From (17) it is obvious that $a_{ij} = 0$ for $i \neq j$, $i = N_{vi} + 1, \dots, N_v$, $j = 1, \dots, N_v$. Hence, the off-diagonal entries of A are non-positive.

The inequality (27) follows immediately from (17), (18), and the positive definiteness of \mathbb{D}_K .

(iii) We now show that A_{11} defined in (17) is an M -matrix. Notice that the non-negativeness of the row sums of A and the properties (26) and (27) imply that A_{11} is diagonally dominant. In theory, we can show that A_{11} is an M -matrix by proving it is irreducible [67]. However, we will need to assume that any pair of interior vertices is connected at least by an interior edge path [18]. To avoid this additional restriction on the mesh, we instead opt to show A_{11} is symmetric and positive definite, which together with (26) and (27) implies that A_{11} is an M -matrix [67].

From (18) it is obvious that A_{11} is symmetric. It suffices to show A_{11} is positive definite. From the strictly positive definiteness of the diffusion matrix \mathbb{D} , there exists a positive constant β such that

$$\mathbb{D}_K \geq \beta \mathbf{I}, \quad \forall K \in \mathcal{T}_h.$$

For any vector $\mathbf{v} = (v_1, \dots, v_{N_{vi}})^T$, we define $v^h = \sum_{i=1}^{N_{vi}} v_i \phi_i \in U_0^h$. From the definition of A_{11} and the fact that $\nabla v^h|_K$ is constant on K , we have

$$\begin{aligned} \mathbf{v}^T A_{11} \mathbf{v} &= \sum_{K \in \mathcal{T}_h} |K| (\nabla v^h|_K)^T \mathbb{D}_K \nabla v^h|_K \\ &\geq \beta \sum_{K \in \mathcal{T}_h} |K| (\nabla v^h|_K)^T \nabla v^h|_K \\ &= \beta \sum_{K \in \mathcal{T}_h} \int_K (\nabla v^h)^T \nabla v^h d\mathbf{x} \\ &= \beta \int_{\Omega} (\nabla v^h)^T \nabla v^h d\mathbf{x} \\ &\geq \beta C_p \int_{\Omega} |v^h|^2 d\mathbf{x}, \end{aligned}$$

where in the last step we have used Poincaré's inequality and $C_p > 0$ is the associated constant. For

any nonzero vector \mathbf{v} , $v^h = \sum_{i=1}^{N_{vi}} v_i \phi_i \not\equiv 0$ and is piecewise linear and continuous on Ω . Consequently,

$$\mathbf{v}^T A_{11} \mathbf{v} \geq \beta C_p \int_{\Omega} |v^h|^2 d\mathbf{x} > 0, \quad \forall \mathbf{v} \neq 0$$

which implies that A_{11} is positive definite. Hence, A_{11} is an M -matrix.

(iv) From (17) it is easy to verify that the inverse of A is given by

$$A^{-1} = \begin{bmatrix} A_{11}^{-1} & -A_{11}^{-1} A_{12} \\ 0 & I \end{bmatrix}.$$

Then (26) and the fact $A_{11}^{-1} \geq 0$ imply that $A^{-1} \geq 0$ and therefore A is an M -matrix.

We have shown above that A is an M -matrix and has non-negative row sums. By Lemma 1.2 we conclude that the linear FEM satisfies DMP when the simplicial mesh satisfies (24). \square

Remark 2.1 For the isotropic case where $\mathbb{D} = a(\mathbf{x})\mathbf{I}$ for some scalar function $a(\mathbf{x})$, condition (24) reduces to the well known non-obtuse angle condition [8, 15]

$$\mathbf{q}_i^K \cdot \mathbf{q}_j^K \leq 0, \quad \forall i \neq j, \forall K \in \mathcal{T}_h, \quad (30)$$

which requires the dihedral angles α_{ij} (cf. (22)) of all mesh elements be non-obtuse. Thus, condition (24) is a generalization of the non-obtuse angle condition. An alternative interpretation of (24) is that the dihedral angles of element K , measured in the Riemannian metric \mathbb{D}_K (piecewise constant), are non-obtuse. \square

Remark 2.2 It is interesting to point out that an explicit mesh condition similar to (24) is obtained by Eigestad et al. [20] for a multipoint flux approximation (MPFA) finite volume method on triangular meshes for anisotropic homogeneous media (i.e., \mathbb{D} is constant). Moreover, (24) reduces to a mesh condition obtained by Li et al. [50] for a similar situation with constant \mathbb{D} and triangular meshes. To see this, let the eigen-decomposition of the constant diffusion matrix \mathbb{D} be

$$\mathbb{D} = \begin{bmatrix} \cos \theta & -\sin \theta \\ \sin \theta & \cos \theta \end{bmatrix} \begin{bmatrix} k_1 & 0 \\ 0 & k_2 \end{bmatrix} \begin{bmatrix} \cos \theta & \sin \theta \\ -\sin \theta & \cos \theta \end{bmatrix}. \quad (31)$$

For an arbitrary triangular element K , denote the angles sharing the edge connecting vertices \mathbf{a}_1 and \mathbf{a}_2 by α and β ; see Fig. 1. Then, a mesh condition of [50] is given by

$$\begin{cases} -k_1 \sin \beta \sin \alpha + k_2 \cos \beta \cos \alpha \leq 0, \\ -k_2 \cos \beta \leq 0, \\ -k_2 \cos \alpha \leq 0, \end{cases} \quad (32)$$

provided that the edge connecting \mathbf{a}_1 and \mathbf{a}_2 is parallel to the primary diffusion direction $(\cos \theta, \sin \theta)^T$ (the eigenvector corresponding to the first eigenvalue of \mathbb{D} , k_1). We now show that (24) reduces to (32) for the current situation. Without loss of generality we assume that the primary diffusion

direction and the edge connecting \mathbf{a}_1 and \mathbf{a}_2 are in the direction of the x -axis; cf. Fig. 1. (In this case we have $\theta = 0$.) It is not difficult to obtain

$$\mathbf{q}_1 = c_1 \begin{bmatrix} -\sin \beta \\ -\cos \beta \end{bmatrix}, \quad \mathbf{q}_2 = c_2 \begin{bmatrix} \sin \alpha \\ -\cos \alpha \end{bmatrix}, \quad \mathbf{q}_3 = c_3 \begin{bmatrix} 0 \\ 1 \end{bmatrix},$$

where c_1 , c_2 , and c_3 are positive constants. From these and (31), (24) reduces to

$$\begin{cases} \mathbf{q}_1^T \mathbb{D}_K \mathbf{q}_2 = \mathbf{q}_1^T \mathbb{D} \mathbf{q}_2 = c_1 c_2 (-k_1 \sin \alpha \sin \beta + k_2 \cos \alpha \cos \beta) \leq 0, \\ \mathbf{q}_1^T \mathbb{D}_K \mathbf{q}_3 = \mathbf{q}_1^T \mathbb{D} \mathbf{q}_3 = c_1 c_3 (-k_2 \cos \beta) \leq 0, \\ \mathbf{q}_2^T \mathbb{D}_K \mathbf{q}_3 = \mathbf{q}_2^T \mathbb{D} \mathbf{q}_3 = c_2 c_3 (-k_2 \cos \alpha) \leq 0, \end{cases}$$

which gives (32). \square

It is often more convenient to express the anisotropic non-obtuse angle condition (24) in terms of mapping F_K from \hat{K} to K . Denote the Jacobian matrix of F_K by F'_K . We define the vectors $\hat{\mathbf{q}}_k$, $k = 1, \dots, d+1$ for the reference element \hat{K} as in (20). The chain rule of differentiation implies

$$\nabla \phi_i = (F'_K)^{-T} \nabla_{\xi} \hat{\phi}_i,$$

where $\hat{\phi}_i(\boldsymbol{\xi}) = \phi_i(F_K(\boldsymbol{\xi}))$. From (23), we have

$$\mathbf{q}_i = (F'_K)^{-T} \hat{\mathbf{q}}_i.$$

Inserting this into (24) we obtain the following theorem.

Theorem 2.2 *If the mesh satisfies*

$$\hat{\mathbf{q}}_i^T (F'_K)^{-1} \mathbb{D}_K (F'_K)^{-T} \hat{\mathbf{q}}_j \leq 0, \quad \forall i \neq j, \quad i, j = 1, \dots, d+1, \quad \forall K \in \mathcal{T}_h \quad (33)$$

then the linear finite element scheme (12) for solving BVP (1) and (2) satisfies DMP.

Corollary 2.1 *Suppose that the reference element \hat{K} is taken as a simplex with non-obtuse dihedral angles. If the mesh satisfies*

$$(F'_K)^{-1} \mathbb{D}_K (F'_K)^{-T} = C_K I, \quad \forall K \in \mathcal{T}_h \quad (34)$$

where C_K is a positive constant on K and I is the $d \times d$ identity matrix, then the linear finite element scheme (12) for solving BVP (1) and (2) satisfies DMP.

Proof. Since \hat{K} is a simplex with non-obtuse dihedral angles, we have

$$\hat{\mathbf{q}}_i^T \hat{\mathbf{q}}_j \leq 0, \quad i \neq j, \quad i, j = 1, \dots, d+1.$$

From this it is easy to see that (34) is sufficient for (33) to hold. \square

In the next two sections mesh condition (34) will be used to develop metric tensors accounting for DMP satisfaction and mesh adaptivity. These metric tensors are needed in anisotropic mesh generation. It is emphasized that (34), as well as mesh conditions (24) and (33), can also be used more directly via direct minimization [50, 53] or variational formulation [30] for optimizing the current mesh to improve DMP satisfaction.

3 Anisotropic mesh generation: metric tensor based on DMP satisfaction

In this section we develop a metric tensor for use in anisotropic mesh generation based on mesh condition (34). To this end, we adopt the so-called M -uniform mesh approach [31, 32] where an anisotropic mesh is viewed as an M -uniform mesh or a uniform one in the metric specified by a tensor $M = M(\mathbf{x})$. The tensor, chosen to be symmetric and positive definite, provides the information on the size, shape, and orientation of mesh elements over Ω necessary for the actual implementation of mesh generation. Various formulations of the metric tensor have been developed in the past for anisotropic mesh adaptation; e.g., see [4, 11, 23, 31, 33]. Once a metric tensor has been determined, the corresponding anisotropic meshes can be generated using a variety of techniques including blue refinement [42, 45], directional refinement [58, 59], Delaunay-type triangulation [4, 5, 11, 56], front advancing [24], bubble packing [72], local refinement and modification [3, 6, 17, 28, 60], and variational mesh generation [7, 19, 30, 35, 41, 40, 70]. In this paper we restrict our attention to the determination of a metric tensor for DMP satisfaction, and refer the interested reader to the above mentioned references for meshing strategies.

It is shown in [32] that when the reference element \hat{K} is taken to be equilateral and unitary in volume, a simplicial M -uniform mesh \mathcal{T}_h for a given $M = M(\mathbf{x})$ satisfies

$$\rho_K |K| = \frac{\sigma_h}{N}, \quad \forall K \in \mathcal{T}_h \quad (35)$$

$$\frac{1}{d} \text{tr}((F'_K)^T M_K F'_K) = \det((F'_K)^T M_K F'_K)^{\frac{1}{d}}, \quad \forall K \in \mathcal{T}_h \quad (36)$$

where N is the number of mesh elements, F_K is the affine mapping from \hat{K} to K , F'_K is the Jacobian matrix of F_K , and

$$M_K = \frac{1}{|K|} \int_K M(\mathbf{x}) d\mathbf{x}, \quad \rho_K = \sqrt{\det(M_K)}, \quad \sigma_h = \sum_{K \in \mathcal{T}_h} \rho_K |K|. \quad (37)$$

Condition (35), referred to as *the equidistribution condition*, determines the size of K from ρ_K . The larger ρ_K is, the smaller $|K|$ is. On the other hand, (36), called *the alignment condition*, characterizes the shape and orientation of K in the sense that the principal axes of the circumscribed ellipsoid of K are parallel to the eigenvectors of M_K while their lengths are reciprocally proportional to the square roots of the respective eigenvalues [32].

To determine M from mesh condition (34), we first notice that the left and right sides of (36) represents the arithmetic and geometric means of the eigenvalues of matrix $(F'_K)^T M_K F'_K$, respectively. From the arithmetic-mean geometric-mean inequality, (36) implies that all of the eigenvalues are equal to each other. In other words, $(F'_K)^T M_K F'_K$ is a scalar matrix, i.e.,

$$(F'_K)^T M_K F'_K = \tilde{C}_K I \quad \text{or} \quad (F'_K)^{-1} M_K^{-1} (F'_K)^{-T} = \tilde{C}_K^{-1} I \quad (38)$$

for some constant \tilde{C}_K . A direct comparison of (38) with (34) suggests that the metric tensor M be chosen in the form

$$M_{DMP,K} = \theta_K \mathbb{D}_K^{-1}, \quad \forall K \in \mathcal{T}_h \quad (39)$$

where $\theta = \theta_K > 0$ is an arbitrary piecewise constant function. Thus, any M -uniform mesh associated with a metric tensor in the form (39) satisfies condition (34). The following theorem follows from Corollary 2.1.

Theorem 3.1 *Suppose that the reference element \hat{K} is taken to be equilateral and unitary in volume. For an M -uniform mesh associated with any metric tensor in the form (39), the linear finite element scheme (12) for solving BVP (1) and (2) satisfies DMP.*

Remark 3.1 Since an M -uniform mesh is aligned with the metric tensor M as characterized by the alignment condition (36), we can conclude that when M is chosen in the form (39), a corresponding M -uniform mesh is aligned with the diffusion matrix \mathbb{D} in the sense that the principal axes of the circumscribed ellipsoid of element K are parallel to the eigenvectors of \mathbb{D}_K while their lengths are proportional to the square roots of the respective eigenvalues. As a consequence, the length of K is greater in a faster diffusion direction and smaller in a slower diffusion direction. A small length scale of mesh elements in slow diffusion directions helps reduce numerical dissipation in those directions. \square

Remark 3.2 Note that $\theta = \theta_K$ in (39) is arbitrary. Thus, in addition to satisfying DMP, there is a degree of freedom for the mesh to account for other considerations. In the next section we shall consider mesh adaptation and choose θ_K to minimize a certain error bound. \square

4 Metric tensors based on DMP satisfaction and mesh adaptivity

In this section we develop a metric tensor taking both the satisfaction of DMP and mesh adaptivity into consideration. The metric tensor takes the form (39), with the scalar function $\theta = \theta_K$ being determined to minimize an interpolation error bound. For simplicity, we consider here an error bound for linear Lagrange interpolation. Other interpolation error bounds (e.g., see [32]) can be considered without major modification.

Lemma 4.1 ([32]) *Let $K \subset \mathbb{R}^d$ be a simplicial element and Π_h be the linear Lagrange interpolation operator. Then,*

$$|v - \Pi_h v|_{H^1(K)} \leq C \|(F'_K)^{-1}\| \left[\int_K [\text{tr}((F'_K)^T |H(v)| F'_K)]^2 d\mathbf{x} \right]^{\frac{1}{2}}, \quad \forall v \in H^2(K) \quad (40)$$

where $\|\cdot\|$ denotes the l_2 matrix norm, $H(v)$ is the Hessian of v , and $|H(v)| = \sqrt{H(v)^2}$.

Lemma 4.2 *For any given $d \times d$ symmetric matrix S , there holds that*

$$|\text{tr}(A^T S A)| \leq \text{tr}(A^T A) \|S\|, \quad \forall A \in \mathbb{R}^{d \times d}. \quad (41)$$

If S is further positive definite, then

$$\|S\|^{-1} \text{tr}(A^T S A) \leq \text{tr}(A^T A) \leq \text{tr}(A^T S A) \|S^{-1}\|. \quad (42)$$

Proof. Denote the eigen-decomposition of S by

$$S = Q \Sigma Q^T,$$

where Q is an orthogonal matrix, $\Sigma = \text{diag}(\lambda_1, \dots, \lambda_d)$, and λ_i , $i = 1, \dots, d$ are the eigenvalues of S . Write

$$A^T Q = [\mathbf{v}_1, \dots, \mathbf{v}_d].$$

Then

$$A^T S A = (A^T Q) \Sigma (Q^T A) = [\mathbf{v}_1, \dots, \mathbf{v}_d] \Sigma [\mathbf{v}_1, \dots, \mathbf{v}_d]^T = \sum_i \lambda_i \mathbf{v}_i \mathbf{v}_i^T.$$

It follows that

$$\begin{aligned} |\operatorname{tr}(A^T S A)| &= \left| \sum_i \lambda_i \operatorname{tr}(\mathbf{v}_i \mathbf{v}_i^T) \right| \\ &= \left| \sum_i \lambda_i \|\mathbf{v}_i\|^2 \right| \\ &\leq \sum_i \|\mathbf{v}_i\|^2 \cdot |\lambda|_{\max} \\ &= \operatorname{tr}(A^T A) \|S\|, \end{aligned}$$

which gives (41). Inequality (42) follows from (41) and that

$$\operatorname{tr}(A^T A) = \operatorname{tr}(A^T S^{\frac{1}{2}} S^{-1} S^{\frac{1}{2}} A) \leq \operatorname{tr}(A^T S A) \|S^{-1}\|. \quad (43)$$

□

The scalar function $\theta = \theta_K$ in (39) is determined based on interpolation error bound (40). From the definition of the Frobenius matrix norm, we have

$$\|A\| \leq \|A\|_F = \sqrt{\operatorname{tr}(A^T A)} = \sqrt{\operatorname{tr}(A A^T)}, \quad \forall A \in \mathbb{R}^{d \times d}.$$

Using this, taking squares of both sides of (40), and summing the result over all elements of \mathcal{T}_h , we have

$$\begin{aligned} |u - \Pi_h u|_{H^1(\Omega)}^2 &= \sum_{K \in \mathcal{T}_h} |u - \Pi_h u|_{H^1(K)}^2 \\ &\leq C \sum_{K \in \mathcal{T}_h} \|(F'_K)^{-1}\|^2 \int_K [\operatorname{tr}((F'_K)^T |H(u)| F'_K)]^2 d\mathbf{x} \\ &\leq C \sum_{K \in \mathcal{T}_h} \|(F'_K)^{-1}\|_F^2 \int_K [\operatorname{tr}((F'_K)^T |H(u)| F'_K)]^2 d\mathbf{x} \\ &= C \sum_{K \in \mathcal{T}_h} [\operatorname{tr}((F'_K)^{-1} (F'_K)^{-T})] \int_K [\operatorname{tr}((F'_K)^T |H(u)| F'_K)]^2 d\mathbf{x}. \end{aligned}$$

From Lemma 4.2 it follows that

$$\begin{aligned} &|u - \Pi_h u|_{H^1(\Omega)}^2 \\ &\leq C \sum_{K \in \mathcal{T}_h} [\operatorname{tr}((F'_K)^{-1} \mathbb{D}_K (F'_K)^{-T})] \cdot \|\mathbb{D}_K^{-1}\| \cdot \int_K [\operatorname{tr}((F'_K)^T \mathbb{D}_K^{-1} (F'_K))]^2 \|\mathbb{D}_K |H(u)|\|^2 d\mathbf{x} \\ &= C \sum_{K \in \mathcal{T}_h} |K| \cdot [\operatorname{tr}((F'_K)^{-1} \mathbb{D}_K (F'_K)^{-T})] \cdot [\operatorname{tr}((F'_K)^T \mathbb{D}_K^{-1} (F'_K))]^2 \\ &\quad \times \|\mathbb{D}_K^{-1}\| \cdot \frac{1}{|K|} \int_K \|\mathbb{D}_K |H(u)|\|^2 d\mathbf{x}. \end{aligned} \quad (44)$$

Consider an M -uniform mesh \mathcal{T}_h corresponding to a metric tensor M_K in the form (39). Then, alignment condition (36) reduces to

$$\frac{1}{d} \text{tr}((F'_K)^T \mathbb{D}_K^{-1} F'_K) = \det((F'_K)^T \mathbb{D}_K^{-1} F'_K)^{\frac{1}{d}}. \quad (45)$$

From the arithmetic-mean geometric-mean inequality, (45) implies that all of the eigenvalues of matrix $(F'_K)^T \mathbb{D}_K^{-1} F'_K$ are equal to each other. As a consequence, all of the eigenvalues of the inverse of $(F'_K)^T \mathbb{D}_K^{-1} F'_K$ are equal to each other, which in turn implies

$$\frac{1}{d} \text{tr}((F'_K)^{-1} \mathbb{D}_K (F'_K)^{-T}) = \det((F'_K)^{-1} \mathbb{D}_K (F'_K)^{-T})^{\frac{1}{d}}. \quad (46)$$

Inserting (45) and (46) into (44) and noticing

$$\det((F'_K)^T \mathbb{D}_K^{-1} F'_K) = |K|^2 \det(\mathbb{D}_K)^{-1}, \quad \det((F'_K)^{-1} \mathbb{D}_K (F'_K)^{-T}) = |K|^{-2} \det(\mathbb{D}_K),$$

we have

$$|u - \Pi_h u|_{H^1(\Omega)}^2 \leq C \sum_{K \in \mathcal{T}_h} |K|^{\frac{d+2}{d}} \det(\mathbb{D}_K)^{-\frac{1}{d}} \|\mathbb{D}_K^{-1}\| \cdot \frac{1}{|K|} \int_K \|\mathbb{D}_K |H(u)|\|^2 d\mathbf{x}. \quad (47)$$

Rewrite this bound as

$$|u - \Pi_h u|_{H^1(\Omega)}^2 \leq C \sum_{K \in \mathcal{T}_h} |K|^{\frac{d+2}{d}} B_K, \quad (48)$$

where

$$B_K = \det(\mathbb{D}_K)^{-\frac{1}{d}} \|\mathbb{D}_K^{-1}\| \cdot \frac{1}{|K|} \int_K \|\mathbb{D}_K |H(u)|\|^2 d\mathbf{x}. \quad (49)$$

Notice that $\int_K \|\mathbb{D}_K |H(u)|\|^2 d\mathbf{x}$ and therefore B_K can vanish locally. To ensure the positive definiteness of the metric tensor to be defined, we regularize the above bound with a parameter $\alpha_h > 0$ as

$$|u - \Pi_h u|_{H^1(\Omega)}^2 \leq C \sum_{K \in \mathcal{T}_h} |K|^{\frac{d+2}{d}} [\alpha_h + B_K] = C \alpha_h \sum_{K \in \mathcal{T}_h} |K|^{\frac{d+2}{d}} \left[1 + \frac{1}{\alpha_h} B_K\right]. \quad (50)$$

From Hölder's inequality, we have

$$\begin{aligned} \sum_{K \in \mathcal{T}_h} |K|^{\frac{d+2}{d}} \left[1 + \frac{1}{\alpha_h} B_K\right] &= \sum_{K \in \mathcal{T}_h} \left(|K| \left[1 + \frac{1}{\alpha_h} B_K\right]^{\frac{d}{d+2}}\right)^{\frac{d+2}{d}} \\ &\geq N^{-\frac{2}{d}} \left(\sum_{K \in \mathcal{T}_h} |K| \left[1 + \frac{1}{\alpha_h} B_K\right]^{\frac{d}{d+2}}\right)^{\frac{d+2}{d}}, \end{aligned} \quad (51)$$

with equality in the last step if and only if

$$|K| \left[1 + \frac{1}{\alpha_h} B_K\right]^{\frac{d}{d+2}} = \text{constant}, \quad \forall K \in \mathcal{T}_h. \quad (52)$$

A direct comparison of this with equidistribution condition (35) suggests that the optimal ρ_K be defined as

$$\rho_K = \left[1 + \frac{1}{\alpha_h} B_K\right]^{\frac{d}{d+2}}. \quad (53)$$

From the relation $\rho_K = \sqrt{\det(M_K)}$, we find the optimal θ_K and M_K as

$$\theta_K = \rho_K^{\frac{2}{d}} \det(\mathbb{D}_K)^{\frac{1}{d}} = \left[1 + \frac{1}{\alpha_h} B_K\right]^{\frac{2}{d+2}} \det(\mathbb{D}_K)^{\frac{1}{d}}, \quad (54)$$

$$M_{DMP+adap,K} = \left[1 + \frac{1}{\alpha_h} B_K\right]^{\frac{2}{d+2}} \det(\mathbb{D}_K)^{\frac{1}{d}} \mathbb{D}_K^{-1}, \quad (55)$$

where B_K is defined in (49). With the so-defined metric tensor, the error bound can be obtained from (50) and (51) for a corresponding M -uniform mesh as

$$|u - \Pi_h u|_{H^1(\Omega)} \leq CN^{-\frac{1}{d}} \sqrt{\alpha_h} \sigma_h^{\frac{d+2}{2d}}. \quad (56)$$

To complete the definition, we need to determine the regularization parameter α_h . We follow [31] to define α_h such that

$$\sigma_h \equiv \sum_{K \in \mathcal{T}_h} \rho_K |K| \leq 2|\Omega|, \quad (57)$$

with which roughly 50% of the mesh points are concentrated in regions of large ρ_K . From (53) and Jensen's inequality, we have

$$\begin{aligned} \sigma_h &= \sum_{K \in \mathcal{T}_h} |K| \left[1 + \frac{1}{\alpha_h} B_K\right]^{\frac{d}{d+2}} \\ &\leq \sum_{K \in \mathcal{T}_h} |K| \left[1 + \alpha_h^{-\frac{d}{d+2}} B_K^{\frac{d}{d+2}}\right] \\ &= |\Omega| + \alpha_h^{-\frac{d}{d+2}} \sum_{K \in \mathcal{T}_h} |K| B_K^{\frac{d}{d+2}}. \end{aligned} \quad (58)$$

By requiring the above bound to be less than or equal to $2|\Omega|$, we obtain

$$\alpha_h = \left(\frac{1}{|\Omega|} \sum_{K \in \mathcal{T}_h} |K| B_K^{\frac{d}{d+2}} \right)^{\frac{d+2}{d}}. \quad (59)$$

Combining (56) with (57) and (59) and summarizing the above derivation, we have the following theorem.

Theorem 4.1 *Suppose that the reference element \hat{K} is chosen to be equilateral and unitary in volume. For any M -uniform simplicial mesh corresponding to the metric tensor (55), the linear finite element scheme (12) for solving BVP (1) and (2) satisfies DMP and the interpolation error for the exact solution u is bounded by*

$$|u - \Pi_h u|_{H^1(\Omega)} \leq CN^{-\frac{1}{d}} \left(\sum_{K \in \mathcal{T}_h} |K| B_K^{\frac{d}{d+2}} \right)^{\frac{d+2}{2d}}, \quad (60)$$

where B_K is defined in (49).

It is remarked that the metric tensor (55) (cf. (49)) depends on the second derivatives of the exact solution u which is what we are seeking/approximating. In actual computation, the second derivatives are replaced with approximations obtained with a Hessian recovery technique such as the one of using piecewise quadratic polynomials fitting in least-squares sense to nodal values of the computed solution (e.g., see [31]). A hierarchical basis error estimator can also be used to approximate the Hessian of the exact solution. It is shown in [34] that the least-squares fitting and the hierarchical basis methods work comparably for all considered cases except for one where the diffusion coefficient is discontinuous and the interfaces are predefined in the mesh. In this case, the latter works better than the former since hierarchical basis estimation does not over-concentrate mesh elements near the interfaces. Since our main goal is to study DMP satisfaction instead of the discontinuity of the diffusion coefficient, we choose to use the least squares fitting method for Hessian recovery in our computation due to its simplicity and problem independent feature.

It is interesting to note that the term in the bracket in (60) can be viewed as a Riemann sum of an integral, i.e.,

$$\sum_{K \in \mathcal{T}_h} |K| B_K^{\frac{d}{d+2}} \sim \int_{\Omega} \det(\mathbb{D})^{-\frac{1}{d+2}} \|\mathbb{D}^{-1}\|^{\frac{d}{d+2}} \cdot \|\mathbb{D}|H(u)|\|^{\frac{2d}{d+2}} d\mathbf{x}.$$

Thus, the interpolation error has an asymptotic bound as

$$\begin{aligned} |u - \Pi_h u|_{H^1(\Omega)} &\leq CN^{-\frac{1}{d}} \left(\sum_{K \in \mathcal{T}_h} |K| B_K^{\frac{d}{d+2}} \right)^{\frac{d+2}{2d}} \\ &\sim CN^{-\frac{1}{d}} \left(\int_{\Omega} \det(\mathbb{D})^{-\frac{1}{d+2}} \|\mathbb{D}^{-1}\|^{\frac{d}{d+2}} \cdot \|\mathbb{D}|H(u)|\|^{\frac{2d}{d+2}} d\mathbf{x} \right)^{\frac{d+2}{2d}}. \end{aligned} \quad (61)$$

We emphasize that both the satisfaction of DMP and mesh adaptation (through minimization of an error bound) are taken into account in the definition of metric tensor (55). An interesting question is what the interpolation error bound looks like if mesh adaptation is not taken into consideration. For example, we consider a case $\theta_K = 1$ in (39). This gives the metric tensor

$$M_K = \mathbb{D}_K^{-1}. \quad (62)$$

Recall that the interpolation error is bounded in (48), i.e.,

$$|u - \Pi_h u|_{H^1(\Omega)} \leq C \left(\sum_{K \in \mathcal{T}_h} |K|^{\frac{d+2}{d}} B_K \right)^{\frac{1}{2}}, \quad (63)$$

where B_K is defined in (49). Moreover, for an M -uniform mesh corresponding to this metric tensor the equidistribution condition (35) reduces to

$$\det(\mathbb{D}_K)^{-\frac{1}{2}} |K| = \frac{\sigma_h}{N}, \quad (64)$$

where $\sigma_h = \sum_{K \in \mathcal{T}_h} \det(\mathbb{D}_K)^{-\frac{1}{2}} |K|$. Inserting (64) into (63), we have

$$\begin{aligned}
|u - \Pi_h u|_{H^1(\Omega)} &\leq C \left(\sum_{K \in \mathcal{T}_h} |K| \left(\det(\mathbb{D}_K)^{\frac{1}{2}} \frac{\sigma_h}{N} \right)^{\frac{2}{d}} B_K \right)^{\frac{1}{2}} \\
&= CN^{-\frac{1}{d}} \sigma_h^{\frac{1}{d}} \left(\sum_{K \in \mathcal{T}_h} |K| \det(\mathbb{D}_K)^{\frac{1}{d}} B_K \right)^{\frac{1}{2}} \\
&= CN^{-\frac{1}{d}} \left(\sum_{K \in \mathcal{T}_h} \det(\mathbb{D}_K)^{-\frac{1}{2}} |K| \right)^{\frac{1}{d}} \left(\sum_{K \in \mathcal{T}_h} |K| \det(\mathbb{D}_K)^{\frac{1}{d}} B_K \right)^{\frac{1}{2}}.
\end{aligned}$$

Thus,

$$|u - \Pi_h u|_{H^1(\Omega)} \leq CN^{-\frac{1}{d}} \left(\sum_{K \in \mathcal{T}_h} \det(\mathbb{D}_K)^{-\frac{1}{2}} |K| \right)^{\frac{1}{d}} \left(\sum_{K \in \mathcal{T}_h} |K| \det(\mathbb{D}_K)^{\frac{1}{d}} B_K \right)^{\frac{1}{2}} \quad (65)$$

$$\sim CN^{-\frac{1}{d}} \left(\int_{\Omega} \det(\mathbb{D})^{-\frac{1}{2}} d\mathbf{x} \right)^{\frac{1}{d}} \left(\int_{\Omega} \|\mathbb{D}^{-1}\| \cdot \|\mathbb{D}|H(u)|\|^2 d\mathbf{x} \right)^{\frac{1}{2}}. \quad (66)$$

This is the interpolation error bound for an M -uniform mesh corresponding to metric tensor (62).

From Hölder's inequality, it follows that

$$\left(\sum_{K \in \mathcal{T}_h} |K| B_K^{\frac{d}{d+2}} \right)^{\frac{d+2}{2d}} \leq \left(\sum_{K \in \mathcal{T}_h} \det(\mathbb{D}_K)^{-\frac{1}{2}} |K| \right)^{\frac{1}{d}} \left(\sum_{K \in \mathcal{T}_h} |K| \det(\mathbb{D}_K)^{\frac{1}{d}} B_K \right)^{\frac{1}{2}}.$$

Thus, the solution-dependent factor of bound (60) is small than or equal to that of bound (65). In this sense, $M_{DMP+adapt}$ defined in (55) leads to a more accurate interpolant than M_{DMP} defined in (62) (or (39) with $\theta_K = 1$).

Moreover, from the standard interpolation theory we recall that the interpolation error for a uniform mesh is bounded by

$$|u - \Pi_h u|_{H^1(\Omega)} \leq CN^{-\frac{1}{d}} \left(\int_{\Omega} \|\nabla^2 u\|^2 d\mathbf{x} \right)^{\frac{1}{2}}. \quad (67)$$

It is easy to see that the solution dependent factor in error bound (61) for $M_{DMP+adapt}$ is in the order of $|\nabla^2 u|_{L^{\frac{2d}{d+2}}(\Omega)}$ and those in (66) for M_{DMP} and (67) for a uniform mesh are in the order of $|\nabla^2 u|_{L^2(\Omega)}$. Thus, (61) has the smallest solution dependent factor, an indication of the advantage of using adaptive meshes. On the other hand, the error bounds (61) and (66) depend on the determinant and norm of the diffusion matrix \mathbb{D} and its inverse. This indicates that DMP satisfaction may sacrifice accuracy. Indeed, as we shall see in the next section, the solution error for DMP-bound meshes can sometimes be larger than that for a uniform mesh.

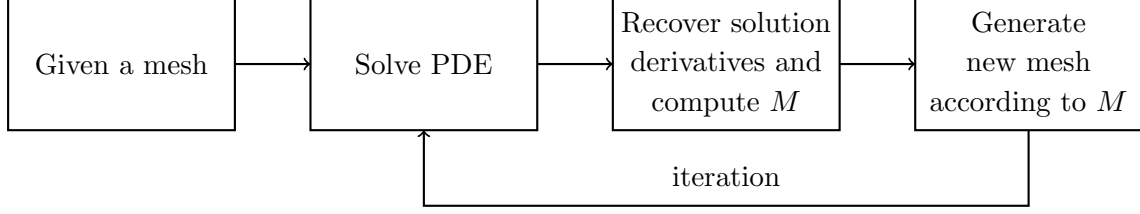


Figure 2: An iterative procedure for adaptive mesh solution of PDEs

5 Numerical results

In this section we present three two-dimensional examples to demonstrate the performance of metric tensors M_{DMP} in (39) with $\theta_K = 1$ based on DMP satisfaction and $M_{DMP+adap}$ in (55) combining DMP satisfaction and mesh adaptivity. For comparison purpose, we also include numerical results obtained with almost uniform meshes (labelled with M_{unif}) and with a metric tensor M_{adap} based on minimization of a bound on the H^1 semi-norm of linear interpolation error [31]:

$$M_{adap,K} = \rho_K^{\frac{2}{d}} \det \left(I + \frac{1}{\alpha_h} |H_K(u)| \right)^{-\frac{1}{d}} \left[I + \frac{1}{\alpha_h} |H_K(u)| \right], \quad (68)$$

where

$$\rho_K = \left\| I + \frac{1}{\alpha_h} |H_K(u)| \right\|_F^{\frac{d}{d+2}} \det \left(I + \frac{1}{\alpha_h} |H_K(u)| \right)^{\frac{1}{d+2}},$$

and α_h is defined implicitly through

$$\sum_{K \in \mathcal{T}_h} |K| \rho_K = 2|\Omega|.$$

Once again, the second derivatives of the exact solution are replaced in actual computation with approximations obtained with a Hessian recovery technique (using piecewise quadratic polynomials fitting in least-squares sense to nodal values of the computed solution [31]).

An iterative procedure for solving PDEs is shown in Fig. 2. In the current computation, each run is stopped after ten iterations. We have found that there is very little improvement in the computed solution after ten iterations for all the examples considered. A new mesh is generated using the computer code BAMG (bidimensional anisotropic mesh generator) developed by Hecht [29] based on a Delaunay-type triangulation method [11]. The code allows the user to supply his/her own metric tensor defined on a background mesh. In our computation, the background mesh has been taken as the most recent mesh available.

Example 5.1 The first example is to consider BVP (1) and (2) with

$$f \equiv 0, \quad \Omega = [0, 1]^2 \setminus \left[\frac{4}{9}, \frac{5}{9} \right]^2, \quad g = 0 \text{ on } \Gamma_{out}, \quad g = 2 \text{ on } \Gamma_{in},$$

where Γ_{out} and Γ_{in} are the outer and inner boundaries of Ω , respectively; see Fig. 3. The diffusion matrix is given by (31) with $k_1 = 1000$, $k_2 = 1$, and θ being the angle of the primary diffusion direction (parallel to the first eigenvector of \mathbb{D}).

This example satisfies the maximum principle and the solution (whose analytical expression is unavailable) stays between 0 and 2. Our goal is to produce a numerical solution which also satisfies DMP and stays between 0 and 2. Moreover, for both cases with a constant and a variable θ we consider, the exact solution has sharp jumps near the inner boundary (cf. Figs. 4 and 8) so mesh adaptation is needed for a proper resolution of them. This example has been studied in [43, 50].

We first consider the case of constant \mathbb{D} with $\theta = \pi/4$. Fig. 4 shows finite element solutions obtained with M_{unif} and $M_{DMP+adap}$. Meshes and solution contours obtained with various metric tensors are shown in Figs. 5 and 6, respectively. No overshoots in the finite element solutions are observed for all cases. However, undershoots and unphysical minima occur in the solutions obtained with M_{unif} ($u_{min} = -0.0602$) and M_{adap} ($u_{min} = -0.0039$) (cf. Fig. 6)(a) and (b)). Fig. 7 shows the decrease of $-u_{min}$ as the mesh is refined. For the range of the number of mesh elements considered, the undershooting improves at a rate of $-u_{min} = O(N^{-0.5})$ for both M_{unif} and M_{adap} . On the other hand, the results confirm the theoretical prediction that the solutions obtained with M_{DMP} and $M_{DMP+adap}$ satisfy DMP and no overshoot/undershoot and no unphysical extremum occur. It should be pointed out that the solution contour obtained with an almost uniform mesh is very smooth but the sharp jumps of the solution are smeared; see Figs. 4(a) and 6(a). The solution contours obtained with M_{DMP} and $M_{DMP+adap}$ are comparable to the one obtained with M_{adap} .

Next we consider a case of variable \mathbb{D} with $\theta = \pi \sin(x) \cos(y)$. The finite element solutions, meshes, and solution contours are shown in Figs. 8, 9, and 10, respectively. Similar observations as for the constant \mathbb{D} case can be made. Especially, undershoots and unphysical extrema occur in the solutions obtained with M_{unif} and M_{adap} but not with M_{DMP} and $M_{DMP+adap}$. Once again, the results confirm our theoretical predictions in the previous sections.

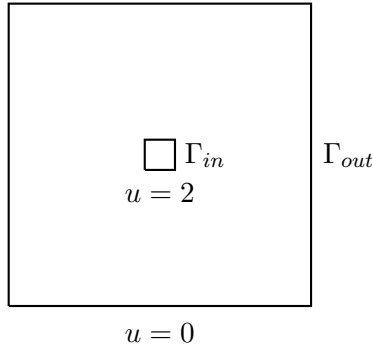


Figure 3: The physical domain and boundary conditions for Example 5.1.

Example 5.2 In this example, we consider BVP (1) and (2) with

$$f \equiv 0, \quad g(x, 0) = g(16, y) = 0,$$

$$g(0, y) = \begin{cases} 0.5y & \text{if } 0 \leq y < 2, \\ 1 & \text{if } 2 \leq y \leq 16, \end{cases} \quad \text{and} \quad g(x, 16) = \begin{cases} 1 & \text{if } 0 \leq x \leq 14, \\ 8 - 0.5x & \text{if } 14 < x \leq 16. \end{cases}$$

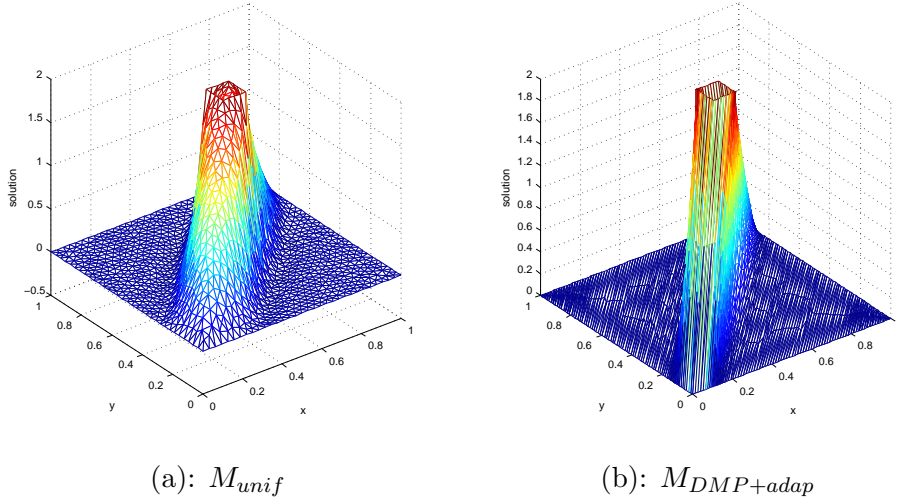


Figure 4: Example 5.1 with constant \mathbb{D} . Finite element solutions obtained with (a) M_{unif} and (b) $M_{DMP+adap}$.

The diffusion matrix is defined as

$$\mathbb{D}(x, y) = \begin{pmatrix} 500.5 & 499.5 \\ 499.5 & 500.5 \end{pmatrix}.$$

This is a simple example with a constant but anisotropic \mathbb{D} and with a continuous boundary condition. It satisfies the maximum principle and its solution stays between 0 and 1.

Numerical solutions, meshes, and solution contours are shown in Figs. 11, 12, and 13, respectively. For this example, both undershoots and overshoots are observed in the computed solutions with M_{unif} and M_{adap} but not with M_{DMP} and $M_{DMP+adap}$. This example demonstrates that a scheme violating DMP can produce unphysical extrema even for a simple problem with constant diffusion, continuous boundary conditions, and a convex domain.

Example 5.3 This example is given by (1) and (2) with

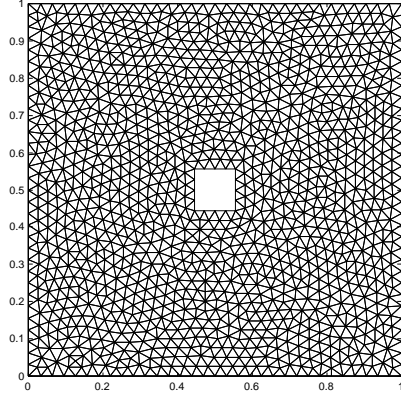
$$\Omega = (0, 1) \times (0, 1), \quad f(x, y) = \begin{cases} 4.0, & \text{if } x < 0.5 \\ -5.6, & \text{if } x > 0.5 \end{cases}, \quad u = u_{exact} \text{ on } \partial\Omega,$$

$$\mathbb{D}(x, y) = \begin{cases} D_1, & \text{if } x < 0.5, \\ D_2, & \text{if } x > 0.5, \end{cases} \quad D_1 = \begin{pmatrix} 1 & 0 \\ 0 & 1 \end{pmatrix}, \quad D_2 = \begin{pmatrix} 10 & 3 \\ 3 & 1 \end{pmatrix}.$$

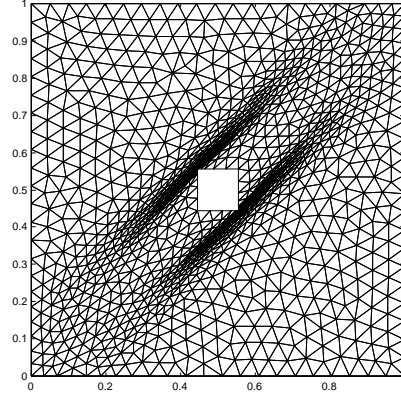
The problem has the exact solution

$$u(x, y) = \begin{cases} 1 - 2y^2 + 4xy + 2y + 6x, & \text{if } x \leq 0.5 \\ -2y^2 + 1.6xy - 0.6x + 3.2y + 4.3, & \text{if } x > 0.5. \end{cases} \quad (69)$$

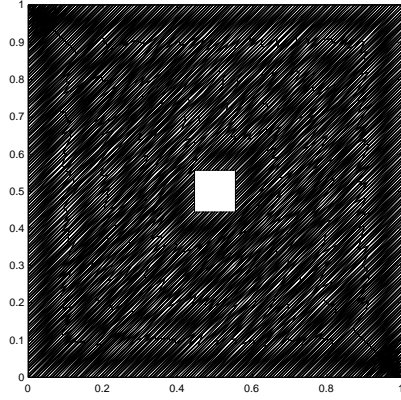
Note that the value and primary diffusion direction of the diffusion matrix change across the line $x = 0.5$. This example has been studied in [43].



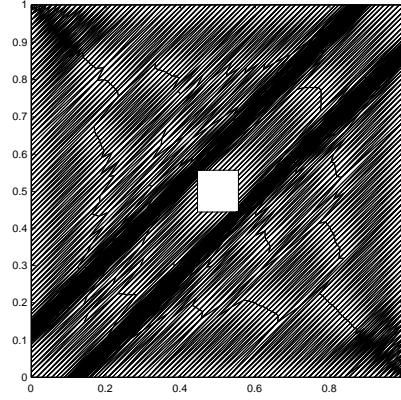
(a): M_{unif} , $N = 2460$



(b): M_{adap} , $N = 2583$



(c): M_{DMP} , $N = 2530$

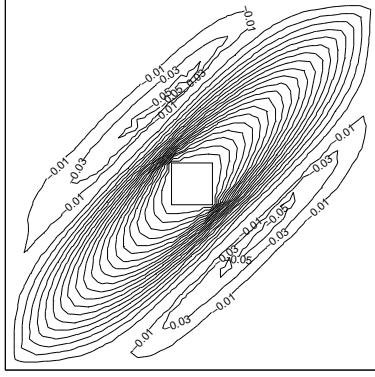


(d): $M_{DMP+adap}$, $N = 2474$

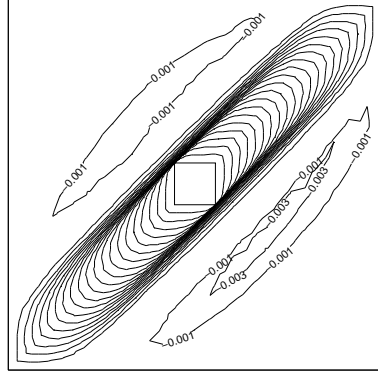
Figure 5: Example 5.1 with constant \mathbb{D} . Meshes obtained with different metric tensors.

Solutions and meshes obtained with various metric tensors are shown in Fig. 14. For this example, no overshoots and undershoots are observed for all numerical solutions. The meshes obtained with M_{DMP} and $M_{DMP+adap}$ show a better alignment with the primary diffusion direction than that obtained with M_{adap} . Moreover, elements are concentrated along the line $x = 0.5$ for the meshes obtained with M_{adap} and $M_{DMP+adap}$ whereas there is no concentration in the mesh shown in Fig. 14(d) for M_{DMP} . The results are consistent with what is expected from the construction of the metric tensors.

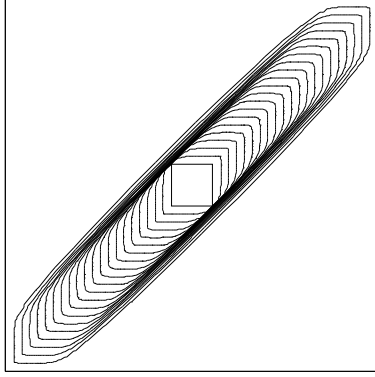
The exact solution is available for this example. The H^1 semi-norm and L^2 norm of the error are shown in Fig. 15 as functions of the number of mesh elements. Metric tensor M_{adap} leads to far more accurate results than the other three metric tensors, which produce comparable results for the considered range of N . Moreover, M_{adap} and $M_{DMP+adap}$ give the same convergence rate, i.e., $|e^h|_{H^1(\Omega)} = O(N^{-0.5})$ and $\|e^h\|_{L^2(\Omega)} = O(N^{-1})$, while M_{unif} and M_{DMP} result in a slower convergence rate, $|e^h|_{H^1(\Omega)} = O(N^{-0.25})$ and $\|e^h\|_{L^2(\Omega)} = O(N^{-0.5})$. This demonstrates the advantage of using adaptive meshes. Interestingly, the results in [43] (Table 4) obtained with a



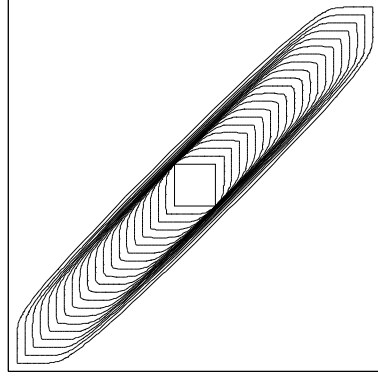
(a): M_{unif} , $u_{min} = -0.0602$



(b): M_{adap} , $u_{min} = -0.0039$



(c): M_{DMP} , $u_{min} = 0$



(d): $M_{DMP+adap}$, $u_{min} = 0$

Figure 6: Example 5.1 with constant \mathbb{D} . Contours of the finite element solutions obtained with different metric tensors.

slope-limited scheme for triangular meshes also show a similar slow convergence.

It should be pointed out that the above results have been obtained when the interface ($x = 0.5$) is not predefined in the mesh. If the interface is predefined in the mesh, then the solution (69) can be approximated accurately in the linear finite element space. As shown in Fig. 16, all metric tensors produce comparable solutions and the same convergence rate $|e^h|_{H^1(\Omega)} = O(N^{-0.5})$ and $\|e^h\|_{L^2(\Omega)} = O(N^{-1})$.

6 Conclusions and comments

In the previous sections we have developed a mesh condition (24) under which the linear finite element approximation of anisotropic diffusion problem (1) and (2) validates the discrete counterpart of the maximum principle satisfied by the continuous problem. The condition is a generalization of

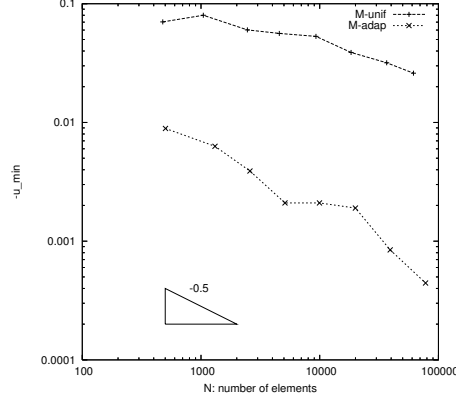


Figure 7: Example 5.1 with constant \mathbb{D} . The undershoot, $-u_{min}$, is shown as functions of the number of elements.

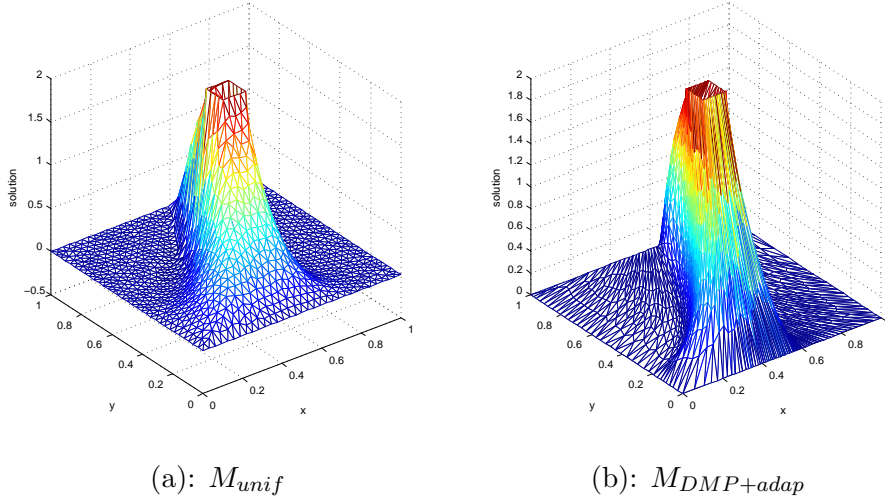
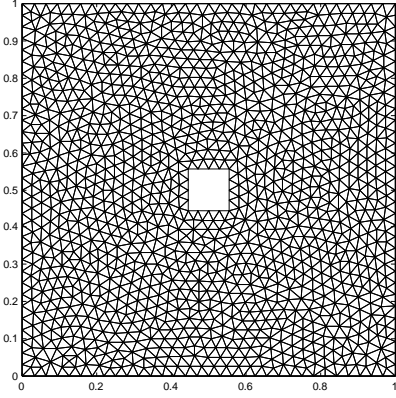


Figure 8: Example 5.1 with variable \mathbb{D} . Finite element solutions obtained with (a) M_{unif} and (b) $M_{DMP+adap}$.

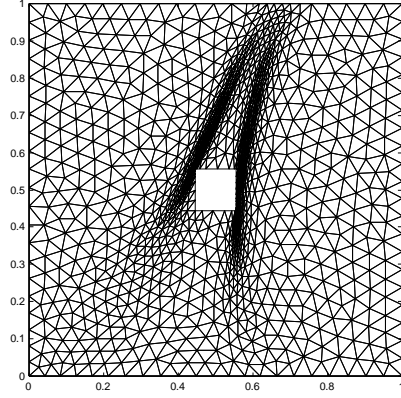
the well known non-obtuse angle condition developed for isotropic diffusion problems and requires that the dihedral angles of mesh elements measured in a metric depending only on the diffusion matrix be non-obtuse.

We have also developed two variants of the anisotropic non-obtuse angle condition, (33) and (34), which can be more convenient to use in actual mesh generation. Indeed, metric tensor (39) for use in anisotropic mesh generation is derived based on (34) for accounting for DMP satisfaction. Moreover, an optimal metric tensor (55) accounting for both DMP satisfaction and mesh adaptation is obtained from (34) by minimizing an interpolation error bound. Features of these metric tensors are illustrated in numerical examples.

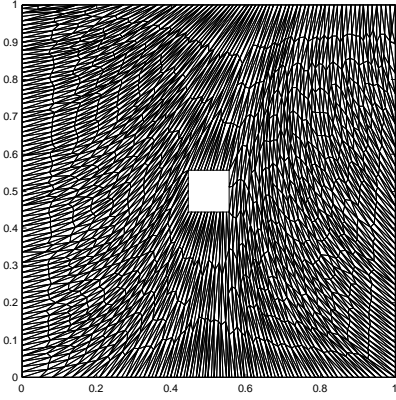
It is worth pointing out that condition (24) has been derived based on the local stiffness matrix on a mesh element. Like the non-obtuse angle condition for isotropic diffusion problems, (24) may be relaxed by considering the global stiffness matrix as a whole [49]. Moreover, we have



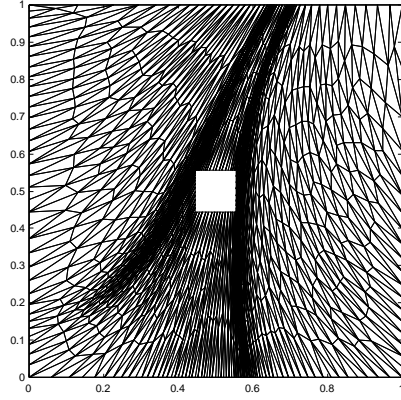
(a): M_{unif} , $N = 2460$



(b): M_{adap} , $N = 2568$



(c): M_{DMP} , $N = 2510$

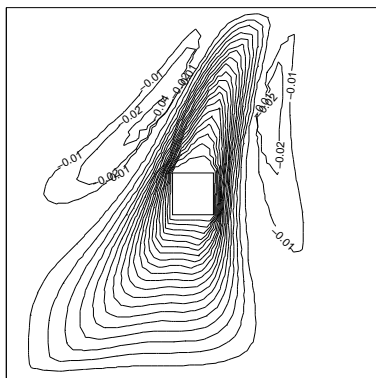


(d): $M_{DMP+adap}$, $N = 2463$

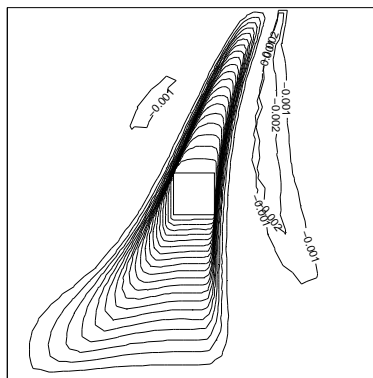
Figure 9: Example 5.1 with variable \mathbb{D} . Meshes obtained from different metric tensors.

restricted our attention to linear PDE (1) and Dirichlet boundary condition (2). But the procedure developed in this work can be extended to problems with nonlinear diffusion $\mathbb{D} = \mathbb{D}(\mathbf{x}, u, \nabla u)$ and mixed boundary conditions (e.g., see [36, 37, 38, 44]) without major modification.

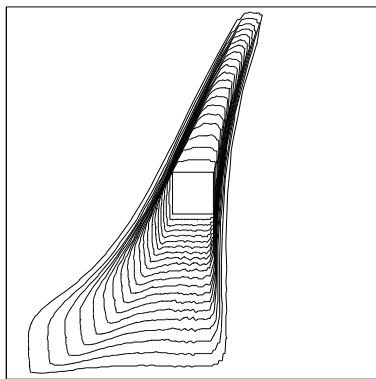
Although the numerical examples have been presented in 2D, the anisotropic non-obtuse angle condition (24) and the corresponding metric tensor formulas (39), (55), and (62) are d -dimensional ($d = 1, 2, 3$). In 3D, a Delaunay triangulation may not guarantee the satisfaction of DMP [49]. Nevertheless, some polyhedrons can be decomposed into tetrahedra satisfying the non-obtuse angle condition (30) and therefore the numerical solution satisfies DMP; e.g., see [44]. It is expected that this will also work for the anisotropic non-obtuse angle condition (24) for a given metric tensor M . On the other hand, the existence of the decomposition of an arbitrary polyhedron into non-obtuse tetrahedra is an open problem [44]. It is also unclear if a 3D triangulation can be generated to (approximately) satisfy the M -uniform mesh conditions (35 and 36). Those are interesting topics to investigate in the future.



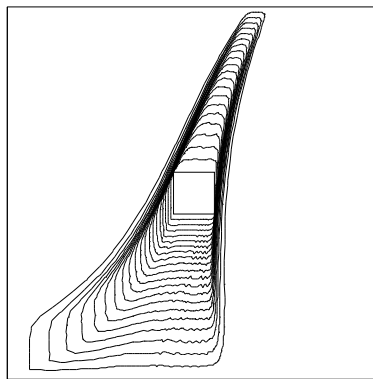
(a): M_{unif} , $u_{min} = -0.0506$



(b): M_{adap} , $u_{min} = -0.0039$



(c): M_{DMP} , $u_{min} = 0$



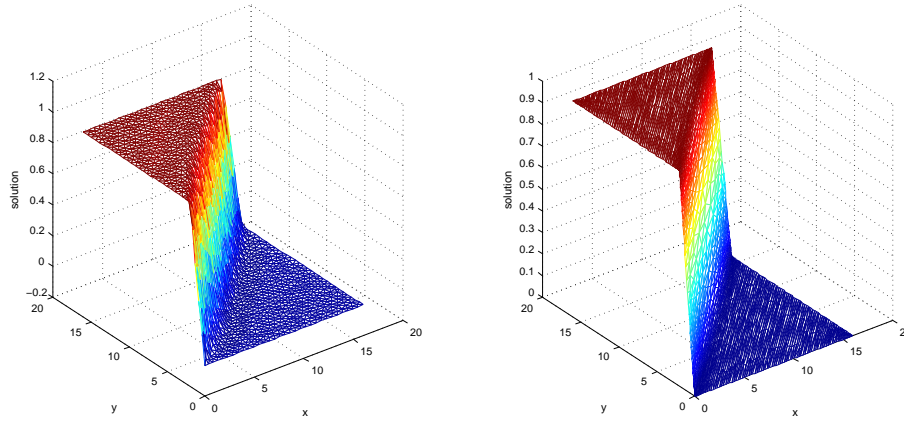
(d): $M_{DMP+adap}$, $u_{min} = 0$

Figure 10: Example 5.1 with variable \mathbb{D} . Contours of the finite element solutions obtained with different metric tensors.

Acknowledgment. The work was supported in part by the National Science Foundation (USA) under grant DMS-0712935.

References

- [1] I. Aavatsmark, T. Barkve, Ø. Bøe, and T. Mannseth. Discretization on unstructured grids for inhomogeneous, anisotropic media. I. Derivation of the methods. *SIAM J. Sci. Comput.*, 19:1700–1716 (electronic), 1998.
- [2] I. Aavatsmark, T. Barkve, Ø. Bøe, and T. Mannseth. Discretization on unstructured grids for inhomogeneous, anisotropic media. II. Discussion and numerical results. *SIAM J. Sci. Comput.*, 19:1717–1736 (electronic), 1998.

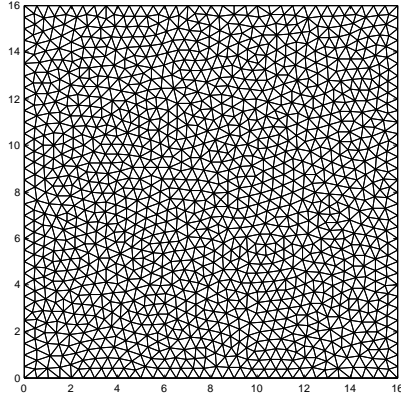


(a): M_{adap} , $u_{min} = -0.0195$

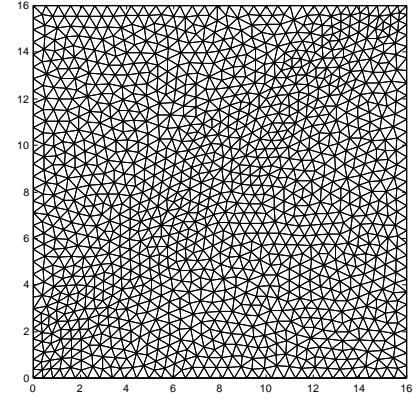
(b): $M_{DMP+adap}$, $u_{min} = 0$

Figure 11: Example 5.2. Finite element solutions obtained with (a) M_{adap} and (b) $M_{DMP+adap}$.

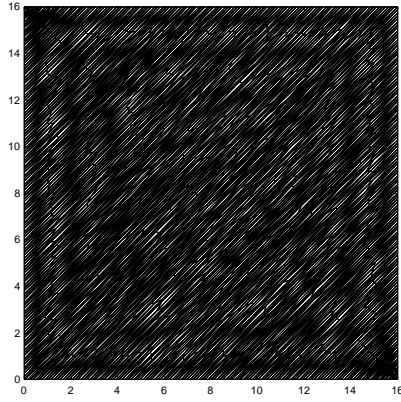
- [3] D. Ait-Ali-Yahia, G. Baruzzi, W. G. Habashi, M. Fortin, J. Dompierre, and M.-G. Vallet. Anisotropic mesh adaptation: towards user-independent, mesh-independent and solver-independent CFD. Part II: Structured grids. *Int. J. Numer. Meth. Fluids*, 39:657–673, 2002.
- [4] H. Borouchaki, P. L. George, P. Hecht, P. Laug, and E. Saletl. Delaunay mesh generation governed by metric specification: Part I. Algorithms. *Fin. Elem. Anal. Des.*, 25:61–83, 1997.
- [5] H. Borouchaki, P. L. George, and B. Mohammadi. Delaunay mesh generation governed by metric specification: Part II. Applications. *Fin. Elem. Anal. Des.*, 25:85–109, 1997.
- [6] F. J. Bossen and P. S. Heckbert. A pliant method for anisotropic mesh generation. In *Proceedings, 5th International Meshing Roundtable*, pages 63–74, Sandia National Laboratories, Albuquerque, NM, 1996. Sandia Report 96-2301.
- [7] J. U. Brackbill and J. S. Saltzman. Adaptive zoning for singular problems in two dimensions. *J. Comput. Phys.*, 46:342–368, 1982.
- [8] J. Brandts, S. Korotov, and M. Křížek. Dissection of the path-simplex in \mathbb{R}^n into n path-subsimplices. *Lin. Alg. Appl.*, 421:382–393, 2007.
- [9] J. Brandts, S. Korotov, and M. Křížek. The discrete maximum principle for linear simplicial finite element approximations of a reaction-diffusion problem. *Lin. Alg. Appl.*, 429:2344–2357, 2008.
- [10] E. Burman and A. Ern. Discrete maximum principle for Galerkin approximations of the Laplace operator on arbitrary meshes. *C. R. Acad. Sci. Paris, Ser.I* 338:641–646, 2004.
- [11] M. J. Castro-Díaz, F. Hecht, B. Mohammadi, and O. Pironneau. Anisotropic unstructured mesh adaption for flow simulations. *Int. J. Numer. Meth. Fluids*, 25:475–491, 1997.



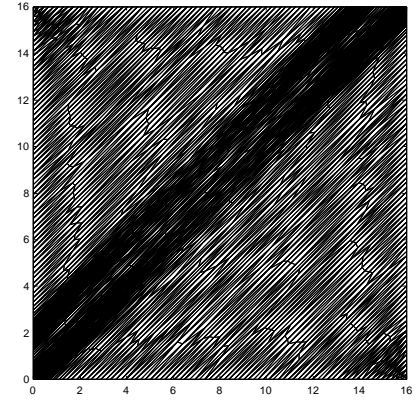
(a): M_{unif} , $N = 2480$



(b): M_{adap} , $N = 2480$



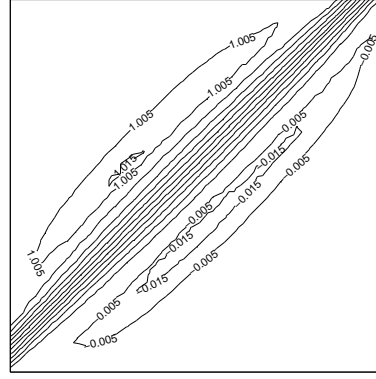
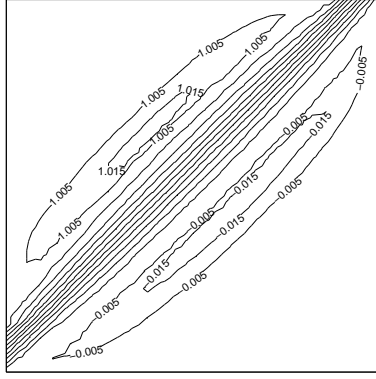
(c): M_{DMP} , $N = 2754$



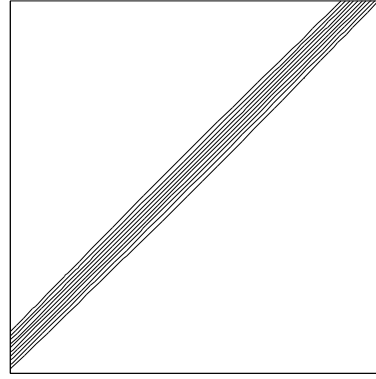
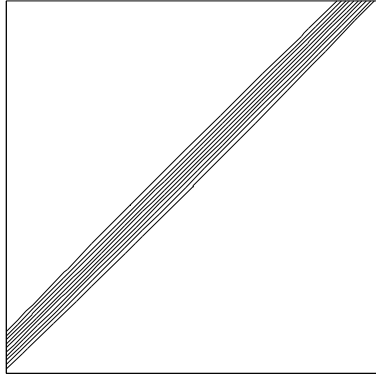
(d): $M_{DMP+adap}$, $N = 2529$

Figure 12: Example 5.2. The adaptive meshes obtained with various metric tensors.

- [12] T. F. Chan and J. Shen. Non-texture inpainting by curvature driven diffusions (CDD). *J. Vis. Commun. Image Rep*, 12:436–449, 2000.
- [13] T. F. Chan, J. Shen, and L. Vese. Variational PDE models in image processing. *Not. AMS J.*, 50:14–26, 2003.
- [14] P. G. Ciarlet. Discrete maximum principle for finite difference operators. *Aequationes Math.*, 4:338–352, 1970.
- [15] P. G. Ciarlet and P.-A. Raviart. Maximum principle and uniform convergence for the finite element method. *Comput. Meth. Appl. Mech. Eng.*, 2:17–31, 1973.
- [16] P. I. Crumpton, G. J. Shaw, and A. F. Ware. Discretisation and multigrid solution of elliptic equations with mixed derivative terms and strongly discontinuous coefficients. *J. Comput. Phys.*, 116:343–358, 1995.



(a): M_{unif} , $u_{min} = -0.0280$, $u_{max} = 1.0209$ (b): M_{adap} , $u_{min} = -0.0195$, $u_{max} = 1.0160$



(c): M_{DMP} , $u_{min} = 0$, $u_{max} = 0$ (d): $M_{DMP+adap}$, $u_{min} = 0$, $u_{max} = 0$

Figure 13: Example 5.2. Contours of the finite element solutions obtained with different metric tensors.

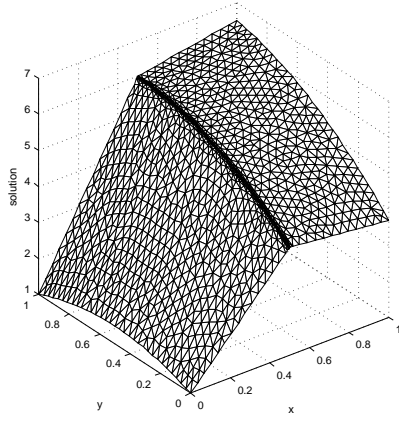
- [17] J. Dompierre, M.-G. Vallet, Y. Bourgault, M. Fortin, and W. G. Habashi. Anisotropic mesh adaptation: towards user-independent, mesh-independent and solver-independent CFD. Part III: Unstructured meshes. *Int. J. Numer. Meth. Fluids*, 39:675–702, 2002.
- [18] A. Drăgănescu, T. F. Dupont, and L. R. Scott. Failure of the discrete maximum principle for an elliptic finite element problem. *Math. Comp.*, 74:1–23, 2004.
- [19] A. S. Dvinsky. Adaptive grid generation from harmonic maps on riemannian manifolds. *J. Comput. Phys.*, 95:450–476, 1991.
- [20] G. T. Eigestad, I. Aavatsmark, and M. Espedal. Symmetry and M -matrix issues for the O -method on an unstructured grid. *Comput. Geosci.*, 6:381–404, 2002.
- [21] A. Ern and J. L. Guermond. *Theory and Practice of Finite Elements*. Springer-Verlag, New York, 2004.

- [22] T. Ertekin, J. H. Abou-Kassem, and G. R. King. *Basic Applied Reservoir Simulation*. SPE textbook series, Vol. 7, Richardson, Texas, 2001.
- [23] P. Frey and P. L. George. *Mesh Generation: Application to Finite Elements*. Hermes Science, Oxford and Paris, 2000.
- [24] R. V. Garimella and M. S. Shephard. Boundary layer meshing for viscous flows in complex domain. In *Proceedings, 7th International Meshing Roundtable*, pages 107–118, Sandia National Laboratories, Albuquerque, NM, 1998.
- [25] S. Günter and K. Lackner. A mixed implicit-explicit finite difference scheme for heat transport in magnetised plasmas. *J. Comput. Phys.*, 228:282–293, 2009.
- [26] S. Günter, K. Lackner, and C. Tichmann. Finite element and higher order difference formulations for modelling heat transport in magnetised plasmas. *J. Comput. Phys.*, 226:2306–2316, 2007.
- [27] S. Günter, Q. Yu, J. Kruger, and K. Lackner. Modelling of heat transport in magnetised plasmas using non-aligned coordinates. *J. Comput. Phys.*, 209:354–370, 2005.
- [28] W. G. Habashi, J. Dompierre, Y. Bourgault, D. Ait-Ali-Yahia, M. Fortin, and M.-G. Vallet. Anisotropic mesh adaptation: towards user-independent, mesh-independent and solver-independent CFD. Part I: General principles. *Int. J. Numer. Meth. Fluids*, 32:725–744, 2000.
- [29] F. Hecht. Bidimensional anisotropic mesh generator. Technical report, INRIA, Rocquencourt, 1997. Source code: <http://www.ann.jussieu.fr/~hecht/ftp/bamg/>.
- [30] W. Huang. Variational mesh adaptation: isotropy and equidistribution. *J. Comput. Phys.*, 174:903–924, 2001.
- [31] W. Huang. Metric tensors for anisotropic mesh generation. *J. Comput. Phys.*, 204:633–665, 2005.
- [32] W. Huang. Mathematical principles of anisotropic mesh adaptation. *Comm. Comput. Phys.*, 1:276–310, 2006.
- [33] W. Huang and X. P. Li. An anisotropic mesh adaptation method for the finite element solution of variational problems. *Fin. Elem. Anal. Des.*, 46:61–73, 2010.
- [34] W. Huang and L. Kamenski and J. Lang. A new anisotropic mesh adaptation method based upon hierarchical a posteriori error estimates. *J. Comput. Phys.*, 229:2179–2198, 2010.
- [35] Olivier-P. Jacquotte. A mechanical model for a new grid generation method in computational fluid dynamics. *Comput. Meth. Appl. Mech. Engrg.*, 66:323–338, 1988.
- [36] J. Karátson and S. Korotov. Discrete maximum principles for finite element solutions of nonlinear elliptic problems with mixed boundary conditions. *Numer. Math.*, 99:669–698, 2005.
- [37] J. Karátson and S. Korotov. Discrete maximum principles for finite element solutions of some mixed nonlinear elliptic problems using quadratures. *J. Comput. Appl. Math.*, 192:75–88, 2006.

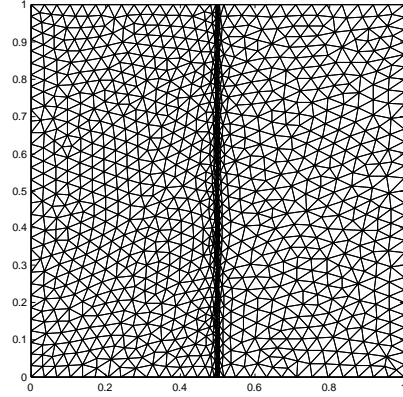
- [38] J. Karátson, S. Korotov, and M. Křížek. On discrete maximum principles for nonlinear elliptic problems. *Math. Comput. Sim.*, 76:99–108, 2007.
- [39] D. A. Karras and G. B. Mertzios. New PDE-based methods for image enhancement using SOM and Bayesian inference in various discretization schemes. *Meas. Sci. Technol.*, 20:104012, 2009.
- [40] P. Knupp, L. Margolin, and M. Shashkov. Reference jacobian optimization-based rezone strategies for arbitrary lagrangian eulerian methods. *J. Comput. Phys.*, 176:93–128, 2002.
- [41] P. M. Knupp. Jacobian-weighted elliptic grid generation. *SIAM J. Sci. Comput.*, 17:1475–1490, 1996.
- [42] R. Kornhuber and R. Roitzsch. On adaptive grid refinement in the presence of internal or boundary layers. *IMPACT Comput. Sci. Engrg.*, 2:40–72, 1990.
- [43] D. Kuzmin, M. J. Shashkov, and D. Svyatskiy. A constrained finite element method satisfying the discrete maximum principle for anisotropic diffusion problems. *J. Comput. Phys.*, 228:3448–3463, 2009.
- [44] M. Křížek and Q. Lin. On diagonal dominance of stiffness matrices in 3D. *East-West J. Numer. Math.*, 3:59–69, 1995.
- [45] J. Lang. An adaptive finite element method for convection-diffusion problems by interpolation techniques. Technical Report TR 91-4, Konrad-Zuse-Zentrum Berlin, 1991.
- [46] C. Le Potier. Schéma volumes finis monotone pour des opérateurs de diffusion fortement anisotropes sur des maillages de triangles non structurés. *C. R. Math. Acad. Sci. Paris*, 341:787–792, 2005.
- [47] C. Le Potier. A nonlinear finite volume scheme satisfying maximum and minimum principles for diffusion operators. *Int. J. Finite Vol.*, 6:20, 2009.
- [48] C. Le Potier. Un schéma linéaire vérifiant le principe du maximum pour des opérateurs de diffusion très anisotropes sur des maillages déformés. *C. R. Math. Acad. Sci. Paris*, 347:105–110, 2009.
- [49] F. W. Letniowski. Three-dimensional delaunay triangulations for finite element approximations to a second-order diffusion operator. *SIAM J. Sci. Stat. Comput.*, 13:765–770, 1992.
- [50] X. P. Li, D. Svyatskiy, and M. Shashkov. Mesh adaptation and discrete maximum principle for 2D anisotropic diffusion problems. Technical report, LANL, 2007. Final Report of the Summer Student Program.
- [51] K. Lipnikov, M. Shashkov, D. Svyatskiy, and Yu. Vassilevski. Monotone finite volume schemes for diffusion equations on unstructured triangular and shape-regular polygonal meshes. *J. Comput. Phys.*, 227:492–512, 2007.
- [52] R. Liska and M. Shashkov. Enforcing the discrete maximum principle for linear finite element solutions of second-order elliptic problems. *Comm. Comput. Phys.*, 3:852–877, 2008.

- [53] M. J. Mlacnik and L. J. Durlofsky. Unstructured grid optimization for improved monotonicity of discrete solutions of elliptic equations with highly anisotropic coefficients. *J. Comput. Phys.*, 216:337–361, 2006.
- [54] D. Mumford and J. Shah. Optimal approximations by piecewise smooth functions and associated variational problems. *Commun. Pure Appl. Math.*, 42:577–685, 1989.
- [55] K. Nishikawa and M. Wakatani. *Plasma Physics*. Springer-Verlag Berlin Heidelberg, New York, 2000.
- [56] J. Peraire, M. Vahdati, K. Morgan, and O. C. Zienkiewicz. Adaptive remeshing for compressible flow computations. *J. Comput. Phys.*, 72:449–466, 1987.
- [57] P. Perona and J. Malik. Scale-space and edge detection using anisotropic diffusion. *IEEE Trans. Pattern Anal. Mach. Intel.*, 12:629–639, 1990.
- [58] W. Rachowicz. An anisotropic h -type mesh refinement strategy. *Comput. Meth. Appl. Mech. Engrg.*, 109:169–181, 1993.
- [59] W. Rachowicz. An anisotropic h -adaptive finite element method for compressible Navier-Stokes equations. *Comput. Meth. Appl. Mech. Engrg.*, 146:231–252, 1997.
- [60] J. Remacle, X. Li, M. S. Shephard, and J. E. Flaherty. Anisotropic adaptive simulation of transient flows using discontinuous Galerkin methods. *Int. J. Numer. Meth. Engrg.*, 62:899–923, 2003.
- [61] P. Sharma and G.W. Hammett. Preserving monotonicity in anisotropic diffusion. *J. Comput. Phys.*, 227:123–142, 2007.
- [62] D. M. Y. Sommerville. *An Introduction to the Geometry of n Dimensions*. Methuen & Co. LTD., London, 1929.
- [63] T.H. Stix. *Waves in Plasmas*. Amer. Inst. Phys., New York, 1992.
- [64] G. Stoyan. On a maximum principle for matrices, and on conservation of monotonicity. With applications to discretization methods. *Z. Angew. Math. Mech.*, 62:375–381, 1982.
- [65] G. Stoyan. On maximum principles for monotone matrices. *Lin. Alg. Appl.*, 78:147–161, 1986.
- [66] G. Strang and G. J. Fix. *An Analysis of the Finite Element Method*. Prentice Hall, Englewood Cliffs, NJ, 1973.
- [67] R. S. Varga. *Matrix Iterative Analysis*. Prentice-Hall, New Jersey, 1962.
- [68] R. S. Varga. On a discrete maximum principle. *SIAM J. Numer. Anal.*, 3:355–359, 1966.
- [69] J. Weickert. *Anisotropic Diffusion in Image Processing*. Teubner-Verlag, Stuttgart, Germany, 1998.
- [70] A. M. Winslow. Adaptive mesh zoning by the equipotential method. Technical Report UCID-19062, Lawrence Livermore Laboratory, 1981. (unpublished).

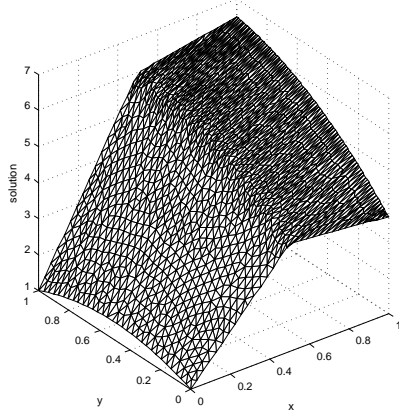
- [71] J. Xu and L. Zikatanov. A monotone finite element scheme for convection-diffusion equations. *Math. Comput.*, 69:1429–1446, 1999.
- [72] S. Yamakawa and K. Shimada. High quality anisotropic tetrahedral mesh generation via ellipsoidal bubble packing. In *Proceedings, 9th International Meshing Roundtable*, pages 263–273, Sandia National Laboratories, Albuquerque, NM, 2000. Sandia Report 2000-2207.



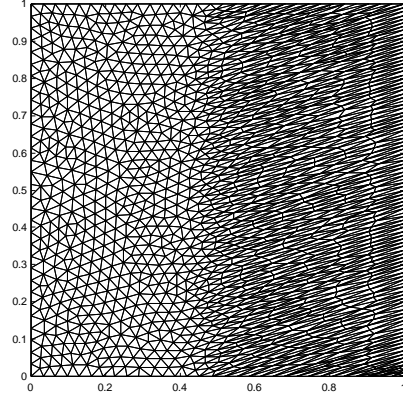
(a): M_{adap} , numerical solution, $u_{min} = 0$



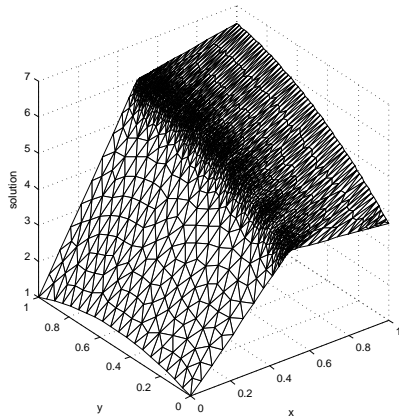
(b): M_{adap} , mesh, $N = 2362$



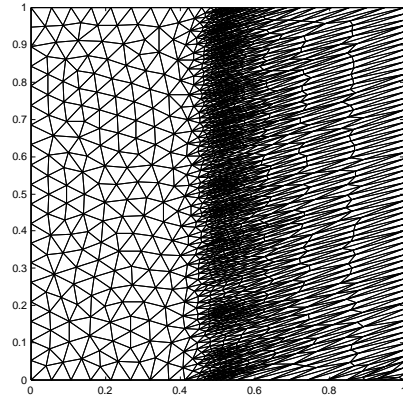
(c): M_{DMP} , numerical solution, $u_{min} = 0$



(d): M_{DMP} , mesh, $N = 2415$

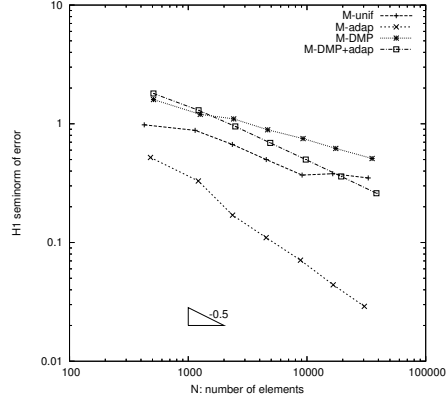


(e): $M_{DMP+adap}$, numerical solution, $u_{min} = 0$

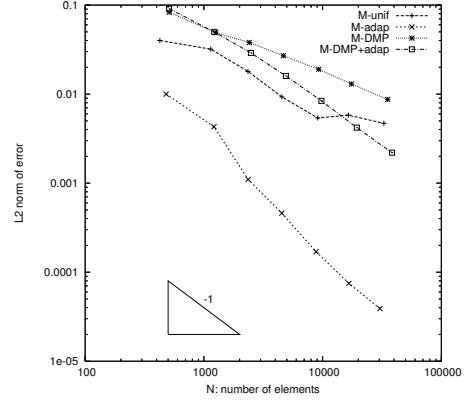


(f): $M_{DMP+adap}$, mesh, $N = 2490$

Figure 14: Example 5.3. Numerical solutions and meshes obtained with three metric tensors.

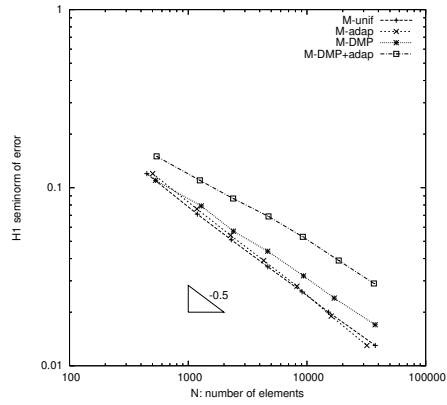


(a): H^1 semi-norm of error

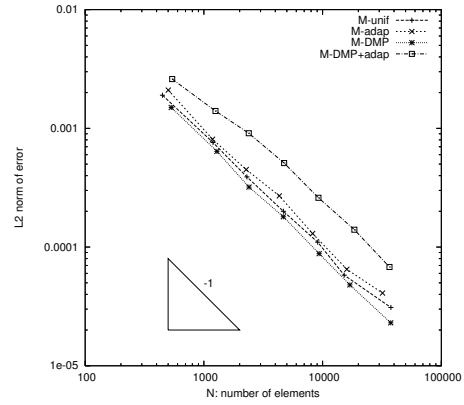


(b): L^2 norm of error

Figure 15: Example 5.3. The H^1 semi-norm and L^2 norm of solution error are shown as functions of the number of elements for metric tensors M_{unif} , M_{adap} , M_{DMP} , and $M_{DMP+adap}$.



(a): H^1 semi-norm of error



(b): L^2 norm of error

Figure 16: Example 5.3. The H^1 semi-norm and L^2 norm of solution error are shown as functions of the number of elements for metric tensors M_{unif} , M_{adap} , M_{DMP} , and $M_{DMP+adap}$. The interface ($x = 0.5$) is predefined in the mesh.